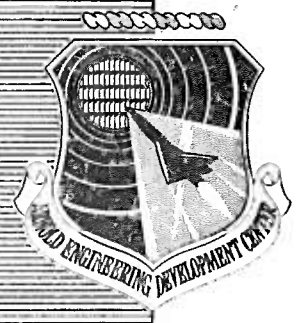

FREE-FLIGHT RANGE TESTS OF THE APOLLO COMMAND MODULE

W. R. Lawrence and W. S. Norman

ARO, Inc.

January 1969

VON KÁRMÁN GAS DYNAMICS FACILITY
ARNOLD ENGINEERING DEVELOPMENT CENTER
AIR FORCE SYSTEMS COMMAND
ARNOLD AIR FORCE STATION, TENNESSEE

NOTICES

When U. S. Government drawings specifications, or other data are used for any purpose other than a definitely related Government procurement operation, the Government thereby incurs no responsibility nor any obligation whatsoever, and the fact that the Government may have formulated, furnished, or in any way supplied the said drawings, specifications, or other data, is not to be regarded by implication or otherwise, or in any manner licensing the holder or any other person or corporation, or conveying any rights or permission to manufacture, use, or sell any patented invention that may in any way be related thereto.

Qualified users may obtain copies of this report from the Defense Documentation Center.

References to named commercial products in this report are not to be considered in any sense as an endorsement of the product by the United States Air Force or the Government.

FREE-FLIGHT RANGE TESTS OF THE APOLLO COMMAND MODULE

W. R. Lawrence and W. S. Norman
ARO, Inc.

FOREWORD

The work reported herein was done at the request of the Arnold Engineering Development Center (AEDC), Air Force Systems Command (AFSC), under System 920E in cooperation with the NASA Manned Spacecraft Center, Houston, Texas.

The test results presented herein were obtained by ARO, Inc. (a subsidiary of Sverdrup & Parcel and Associates, Inc.), contract operator of the AEDC, AFSC, Arnold Air Force Station, Tennessee, under Contract F40600-69-C-0001. The tests were conducted during the period from January 25 to March 10, 1967, under ARO Project No. VT0744, and the manuscript was submitted for publication on September 13, 1968.

This technical report has been reviewed and is approved.

Eugene C. Fletcher
Lt Colonel, USAF
AF Representative, VKF
Directorate of Test

Roy R. Croy, Jr.
Colonel, USAF
Director of Test

ABSTRACT

Results are presented for free-flight range tests of the basic Apollo Command Module configuration (smooth heat shield) conducted in Range G at nominal Mach numbers of 6.0 and 8.5. The Reynolds number based on model diameter and free-stream conditions varied from 50,000 to 240,000. Both drag and stability data are presented in addition to trim angles of attack corresponding to three lateral center-of-gravity positions. Comparison of the results with data from wind tunnels shows at most only small sting effects on the wind tunnel data.

CONTENTS

APPENDIXES

I. ILLUSTRATIONS

Figure

NOMENCLATURE

A	Reference area of model, $\pi d^2/4$
A_1, A_2, A_3	Constants (Eq. (III-2))
C_1, C_2	Constants in representation of pitching moment (Eqs. (IV-23) and (IV-24))
C_A	Axial-force coefficient
C_D	Drag coefficient
C_L	Lift coefficient
C_{L_α}	Lift-force derivative
C_m	Pitching-moment coefficient
C_{m_α}	Pitching-moment derivative
C_{mp_α}, C_{np_α}	Magnus parameters
C_{m_q}, $C_{m_{\dot\alpha}}$	Damping-in-pitch derivatives
C_N	Normal-force coefficient
C_n	Yawing-moment coefficient
C_{n_β}	Yawing-moment derivative
C_y	Side-force coefficient
D	Damping parameter
D_α, D_β	Coefficients of solution (see Eqs. (IV-52) and (IV-53))
d	Diameter of model
e	Amount of center-of-gravity offset (Fig. 2)

F, G	Inertia parameters, defined by Eqs. (IV-3) and (IV-4)
F_1, F_2	Defined by Eq. (IV-44)
I_x, I_y, I_z	Moments of inertia
i	Imaginary unit, $\sqrt{-1}$
$\vec{i}$, $\vec{j}$, $\vec{k}$	Unit vectors in body-fixed system
$\vec{i}_1$, $\vec{j}_1$, $\vec{k}_1$	Unit vectors in nonrolling body axis system
$\vec{i}_r$, $\vec{j}_r$, $\vec{k}_r$	Unit vectors in range system
K_1, K_2, K_3	Defined by Eqs. (IV-33), (IV-34), and (IV-38)
k_a	$\sqrt{I_x/md^2}$
k_t	$\sqrt{I_y/md^2}$
M	Pitching moment
M_∞	Mach number
m	Mass of model
N	Yawing moment
P, Q, R	Roll rate, pitch rate, and yaw rate (usually radians/ft)
P_o	$\frac{(e/d)}{0.03384}$ (see Appendix IV)
q	Dynamic pressure
$Re_{\infty d}$	Reynolds number based on free-stream conditions and diameter of model
Re_{2d}	Reynolds number based on conditions behind normal shock and diameter of model
S	Defined by Eq. (IV-51)
T_1, T_2	Defined by Eqs. (IV-54) and (IV-55)
t	Time
U, V, W	Velocity components relative to body-fixed axis system
U_1, V_1, W_1	Velocity components relative to nonrolling body axis system
V_∞	Velocity of model
x	Axial distance along range
$\bar{x}$	Axial location of center of gravity (Fig. 2)

x, y, z	Body-fixed axis system
x_1, y_1, z_1	Nonrolling body axis system
x_r, y_r, z_r	Range axis system
Y	Side force
$y + iz$	Transverse displacement of model from range axis (see Eq. (III-6))
Z	Force in z direction
Z_1	Defined by Eq. (IV-50)
α	Angle of attack in body-fixed axis system
α_e	Total angle of attack
α_r	Angle of attack in nonrolling axis system
α_t	Trim angle
α_{t_o}	Trim angle for zero roll rate
α_1	$\alpha - \alpha_t$
β	Angle of sideslip in body-fixed axis system
β_r	Angle of sideslip in nonrolling axis system
β_1	Yaw angle in nonrolling body axis system
γ	Cosine α_e
$\overline{\delta}$	Mean total angle of attack (see Eq. (III-9))
$\delta_\alpha, \delta\beta$	Phase shift angles (Eqs. (IV-52) and (IV-53))
θ	Elevation angle
θ_1	Elevation angle in nonrolling body axis system
μ_1, μ_2	See Eq. (III-2)
ξ	Dependent variable in the yaw equation (see Appendix III)
ρ	Range air density
ϕ	Roll angle
ϕ_o	Initial roll angle
ϕ_1', ϕ_2'	See Eq. (III-2)
ω_1, ω_2	See Eq. (IV-49)
ω_A, ω_B	Defined by Eq. (IV-45)

ω_α, ω_β	Defined by Eqs. (IV-30) and (IV-37)
$(\ )'$	$= d(\ )/dx$

SUBSCRIPTS

o, t	Trim conditions
cg	Center of gravity

Note: The coordinate system used in this report has the x axis in the direction of the velocity vector, whereas the coordinate system used in Ref. 1 has the x-axis opposite to the velocity vector. Therefore, α of this report is the supplement of the α of Ref. 1. In addition, C_A, C_m, and C_N are of opposite sign. (See the upper left portion of Fig. IV-4 (Appendix IV) for the positive directions used in this report.)

SECTION I
INTRODUCTION

Initial aerodynamic measurements in the reentry portion of the unmanned Apollo mission AS-202 trajectory indicated several anomalies between flight data and preflight predictions based on ground tests. In an attempt to resolve some of these anomalies, a comprehensive test program was conducted in the test facilities of the von Kármán Gas Dynamics Facility (VKF) (Ref. 1). As part of this investigation, several Apollo models were flight tested in the VKF 1000-ft Hypervelocity Range (G) (Armament Test Cell, Hyperballistic (G)). The primary purpose of these range tests was to determine if sting effects were significant in the wind tunnel tests.

Drag and stability measurements were made at nominal Mach numbers of 6.0 and 8.5 and within a range of free-stream Reynolds numbers, based on the diameter of the model ($Re_{\infty d}$), from 50,000 to 240,000.

The results of the range tests are presented in this report, and the results of the entire VKF investigation are summarized in Ref. 1.

SECTION II
APPARATUS

2.1 RANGE

The variable-density range consists of a 10-ft-diam steel tank and has an 840-ft instrumented length (Fig. 1, Appendix I). The position and attitude of the model during the flight are provided by 43 dual-axis spark shadowgraphs located at nominal 20-ft intervals along the instrumented range length. A digitized film reader is used for numerical interpretation of the shadowgrams. Angular orientation and linear coordinates of most test configurations can be determined to within approximately ±0.25 deg and ±0.002 ft, respectively, at each shadowgraph station. A multichannel digital chronograph records the time of model flight between any two stations to within ±0.2 μsec.

Model launching was accomplished by a two-stage, powder-hydrogen gun having a 2.5-in. bore diameter. A blast chamber which absorbs the expanding muzzle gases constitutes the initial 85 ft of the range and provides sufficient length along the flight trajectory for sabot separation from the model before entry into the range proper.

2.2 MODELS AND SABOTS

The configurations tested corresponded to the Apollo command module with a smooth symmetrical heat shield as shown in Fig. 2. The models were constructed of 4340 steel. Three different internal model geometries were used in order to permit nominal offset center-of-gravity (cg) positions, e/d, of 0, 0.0169, and 0.0338 and corresponding trim angles of approximately 0, 10, and 20 deg, respectively, in flight. The fully offset cg position (e/d = 0.0338) was obtained with the use of two cylindrical inserts, one of Kennertium W2® and the other of LA141A-T7 magnesium-lithium alloy, which were inserted into the body perpendicular to the model centerline and 180 deg apart. Similarly, the partially offset cg position was obtained by using a single magnesium-lithium cylindrical insert. Each cylindrical insert was positioned so that the extension of its longitudinal axis passed through the model longitudinal cg position; therefore, the three different offset cg positions could be obtained without significantly affecting the longitudinal cg position. Minor adjustment of the longitudinal cg position of a model was made by longitudinal movement of a small internal ballast. Center-of-gravity locations of the models were measured to within 0.001 in. in both the transverse and longitudinal directions. Table I of Appendix II presents a summary of the measured physical characteristics of the models.

Four-piece sabots, made of Lexan®, were used to position the models in the approximate trim attitude during the launching. Figure 3 shows the angular alignment of a full-offset model in a portion of its sabot. In this photograph the model has been rotated 90 deg about the longitudinal axis with respect to its launch position in the sabot in order to show more clearly one of the inserts in the model.

In order to determine roll rate during flight independent of the conventional curve-fitting technique, described in Appendixes III and IV, two small pins (not shown in Fig. 3) were inserted into the model apex (base) parallel to the model centerline and approximately 1/8 in. apart. Roll orientation as a function of downrange distance traveled was then obtained by determining the relative pin positions from shadowgram measurements.

SECTION III
PROCEDURE

3.1 LAUNCHING

In range testing, the transverse movement of a free-flight model relative to the range centerline is of concern in ensuring that the model

remains within the view area of the shadowgraph system during the flight. The problem of keeping the model within the view area is magnified for models having offset cg positions and nonzero lift coefficients at the trim condition. The "heavy model" type of construction (steel models) used in this investigation was a significant aid in minimizing this transverse movement.

The sabots used in the present investigation were designed so that the models with offset cg positions were oriented in the launcher at an attitude approximately the same as the anticipated trim angle. Ideally only small-amplitude angular motion would result, and the trim angle of a model in free flight could be determined from the measured model motion quite well. However, in the actual launchings of the models, initial disturbances encountered caused large-amplitude motion in pitch and yaw about the trim angle. Roll measurements obtained with use of the pins previously discussed indicated that the roll rate of each model was approximately constant during its flight.

3.2 DATA REDUCTION

The range data were initially analyzed using the conventional linear analysis procedures of Appendix III. No stability data are presented for models with offset cg positions because it is felt that violations of equation restrictions (discussed in Appendix III) related to the combination of large asymmetries and large-amplitude motion involved were too severe to permit a feasible determination of the stability derivatives for these models.

Typical angular motion plots are given in Fig. 4 for representative cases for each of the cg positions. It is shown that the assumed model for the yaw program (Appendix III) and the values determined by the curve fitting technique give results that match the experimental data very closely. However, the values of the trim angle determined by the program were found to differ from the values based on wind tunnel data. This discrepancy between the wind tunnel and range results was found to be caused by the effect of roll rate on trim angle. The magnitude of this effect is given by Eq. (III-3) of Appendix III and Eq. (IV-31) of Appendix IV. For more typical configurations with higher fineness ratios the difference between the rolling trim angle, α_t, and the nonrolling trim angle, α_{t_o}, tends to be small, with α_{t_o} smaller than α_t. However, in the case of the Apollo configuration, the inertia ratio (I_x/I_y) is greater than 1 and α_{t_o} can be larger than α_t. Further, it follows from Eq. (III-3) that this difference is larger for configurations with large trim angles.

A more complete analysis of the data was made using the second-order technique described in Appendix IV. This technique takes into account a number of additional factors not included in the yaw program. These additional factors are the nonlinearity of the moment curve, the effect of combined angles of attack and sideslip on the moment, and the effects of vehicle asymmetries.

The data analysis techniques used are summarized below.

Parameter	Symmetrical Models	Models with Offset cg
C_D	Drag program (Appendix III)	Drag program (Appendix III)
α_t	Yaw program (Appendix III) (Linear)	Yaw program (Appendix III) and second-order method (Appendix IV)
$C_m/\tan \alpha_e$	Yaw program (Appendix III) (Linear)	Not obtained.
$C_L/\tan \alpha_e$	Swerve program (Appendix III)	Not obtained.

The estimated maximum probable errors in the quantities derived from either the linear or second-order analyses are listed below.

C_D	α_t	$C_m/\tan \alpha_e$	$C_L/\tan \alpha_e$
±1.5 percent	±1.25 deg	±4 percent	±5 percent

3.3 DESCRIPTION OF SHOTS

The physical characteristics of the models are summarized in Table I, and the test conditions and aerodynamic data are summarized in Table II. There were three series of shots. The first series was made with symmetrical models (cg on centerline) at a nominal Mach number of 6. These shots were numbers 600, 601, and 602. Note that the axial location of the cg, $\bar{x}/d$, for these shots was nominally 0.242, rather than 0.270 which was the value for the remainder of the shots. The pitching-moment coefficient data from shots 601 and 602 given in Table II were adjusted to a cg location of 0.270 for comparison with other data. The second series of shots (614 to 620) was made at a nominal Mach number of 8.5, at a range pressure of from 4 to 8 mm Hg, with symmetrical models, models with cg offsets of half the design value, and models with full-offset cg. The last series included shots 631, 632, and 633; the first two of these were made at a higher range pressure.

SECTION IV
RESULTS AND DISCUSSION

The free-flight range measurements, including trim angle, drag coefficient, and stability data are summarized in Table II. The data are presented in Figs. 5 through 8, which also include comparisons with wind tunnel data.

In Fig. 5a, range trim angle values for the free-flight models including roll effects, and trim values corresponding to zero roll, as evaluated using the linear analysis of Appendix III, are presented. Also shown are corresponding wind tunnel trim angle data. It is apparent from the range data that roll effects on the trim angle of an Apollo-type configuration can be significant. Wind tunnel trim angle values (corresponding to nonrolling motion) agree well with the range trim angle measurements adjusted to zero roll on the basis of the conventional linear analysis of Appendix III.

The range trim angle data reduced using the second-order method of Appendix IV are shown in Fig. 5b. They indicate some improvement in the spread of the measurements, but present essentially identical results for average trim angle of a nonrolling model as obtained by use of Eq. (III-3) in the conventional analysis.

With the exception of shot 632, the range data are within ±1 deg of the wind tunnel data. This spread is considered quite reasonable, in view of the rather large-amplitude motions involved. No satisfactory explanation has been found for the apparent deviation in the trim angle of shot 632, although it should be noted that a 0.001-in. shift of cg position would place that data point in a reasonably satisfactory position.

The drag coefficients as a function of effective angle of attack are presented in Fig. 6. Also shown are some wind tunnel data obtained at comparable test conditions. At these relatively high Reynolds numbers ($Re_{2d} > 10^4$) there is no reason to expect a wall temperature effect on the drag coefficient for this blunt shape, so the two sets of data should be directly comparable. At a free-stream Mach number of 6, the data from the wind tunnel and the data from the range are in good agreement. At a free-stream Mach number of 8.5, the drag coefficients from the range are higher than those from the wind tunnel, especially for the higher mean angles of attack. The reason for this difference is not apparent. The wind tunnel data indicate no Mach number effects on the drag coefficient between free-stream Mach numbers of 6 and 8.5, whereas the range data indicate a slight increase. The differences between the

two sets of data are about 3 percent, which is not a large difference, but it is larger than the probable errors for either set of data. Therefore, this difference should be considered as an indication of either a slight sting effect or a difficulty in obtaining drag coefficients for large-amplitude motions at the higher Mach numbers.

The experimental static stability parameter, $C_m/\tan \alpha_e$, obtained for the symmetrical configurations using the linear analysis of Appendix III is presented in Fig. 7a. The values plotted correspond to measurements listed in Table II that have been adjusted to a longitudinal reference point at $\bar{x}/d = 0.270$. The data indicate that the configuration is statically stable at both nominal Mach numbers at which testing was accomplished, and no Mach number effect is discernible.

The $C_L/\tan \alpha_e$ values obtained for the symmetrical configuration are presented in Fig. 7b. The data indicate negative values at both Mach numbers.

Linear curves with slopes corresponding to the reduced range pitching-moment and lift-force derivatives resulting from the analysis of Appendix III are shown for the $M_\infty = 8.5$ range data in Fig. 8 along with wind tunnel C_m and C_L data. The wind tunnel data have been plotted as a function of $\tan \alpha$ which is more appropriate than α as a parameter in making the comparisons with the range measurements. Reasonable agreement is indicated between the range and wind tunnel measurements, considering that the range measurements are for an amplitude range corresponding to $\tan \alpha$ up to about 0.1. It should be noted that the decrease in the absolute magnitude of the parameter $C_L/\tan \alpha_e$ with the mean total angle of attack as shown in Fig. 7b is consistent with the shape of the wind tunnel curve shown in Fig. 8b.

Some rough measurements of the dynamic stability damping parameter were obtained for the symmetrical configuration. The measurements are not presented because their questionable accuracy does not permit attaching more significance to the measurements than making the remark that they indicate near neutral dynamic stability for the Apollo configuration.

It should be noted that no Reynolds number effect is discernible in the limited aerodynamic data of this report. The effect of Reynolds number in wind tunnel tests of the Apollo configuration is discussed in detail in Ref. 1.

SECTION V
CONCLUDING REMARKS

The basic Apollo command module configuration has been tested in the VKF 1000-ft hypervelocity range (G) at nominal Mach numbers of 6 and 8.5 and within a range of Reynolds number (based on model diameter and free-stream conditions) from 50,000 to 240,000. Comparison of the results with data from wind tunnels shows reasonable agreement with the only difference worth noting being that the drag coefficient from the range tests is about 3 percent higher than that from the wind tunnel for high amplitude motions at $M_\infty = 8.5$. Within this extent, sting effects were found to be negligible.

The free-flight range experiments with an offset cg were interesting in that model roll in combination with a large inertia ratio ($(I_X/I_Y) > 1$) decreased the trim angle of the rolling Apollo model significantly. Second-order effects on the trim angle were suspected because of the nonlinear moment characteristics of the Apollo configuration; however, trim angle data on the basis of either the linear yaw analysis or a newly devised second-order analysis indicate similar results.

REFERENCES

1. Griffith, B. J. and Boylan, D. E. "Postflight (AS-202) Apollo Command Module Aerodynamic Simulation Tests." AEDC-TR-67-238 (AD666927), March 1968.

2. Murphy, C. H. "Free-Flight Motion of Symmetric Missiles." BRL-R-1216, July 1963.

3. Scarborough, J. B. Numerical Mathematical Analysis. The Johns Hopkins Press, Baltimore, 1930.

4. Etkin, B. Dynamics of Flight: Stability and Control. John Wiley and Sons, Inc., New York, 1959, p. 116.

5. Cunningham, W. J. Introduction to Nonlinear Analysis. McGraw-Hill, New York, 1958.

APPENDIXES

I. ILLUSTRATIONS
II. TABLES
III. BASIC DATA REDUCTION PROCEDURES FOR RANGE TESTS
IV. SECOND-ORDER THEORY

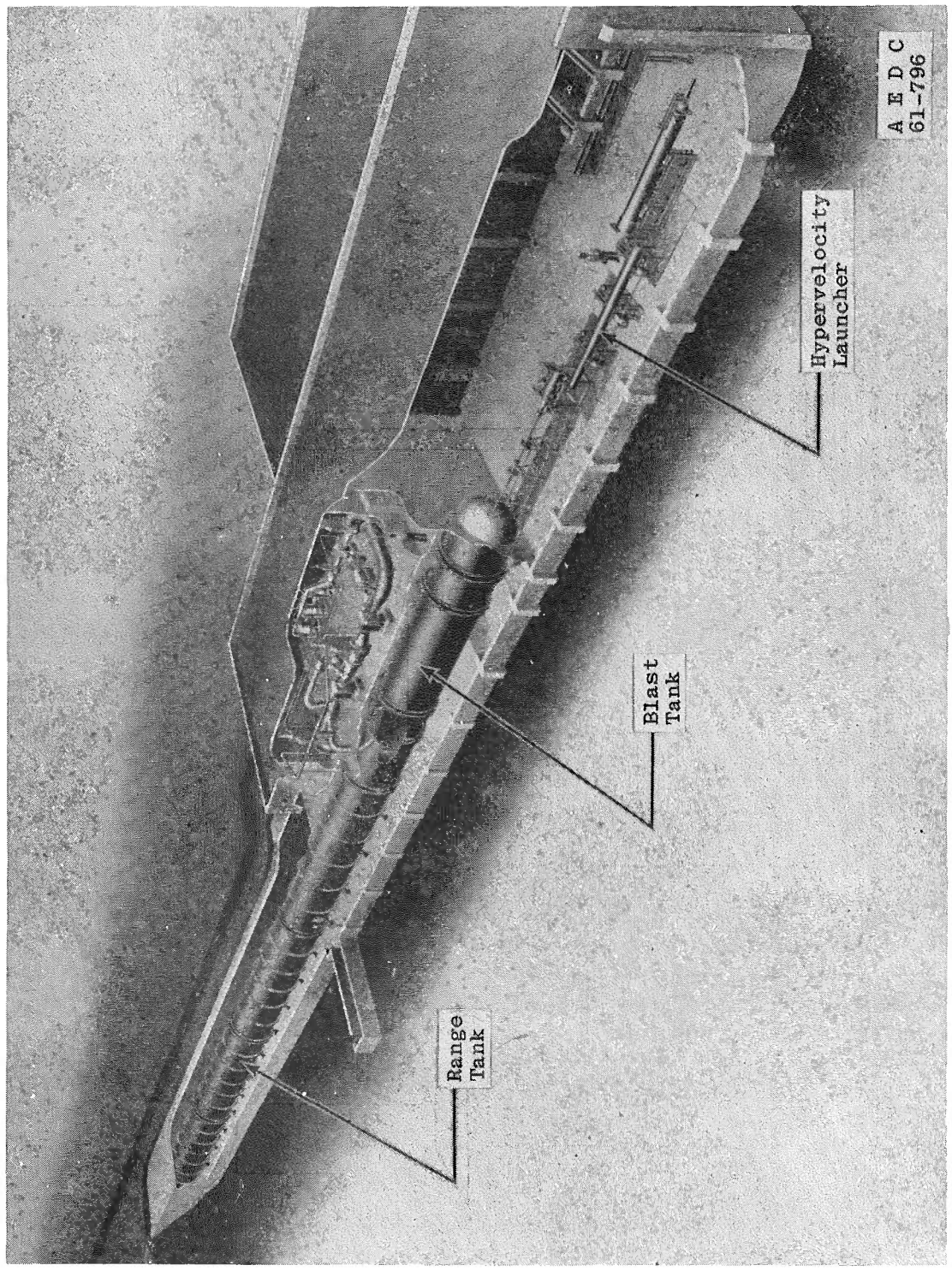

Fig. 1 Range G

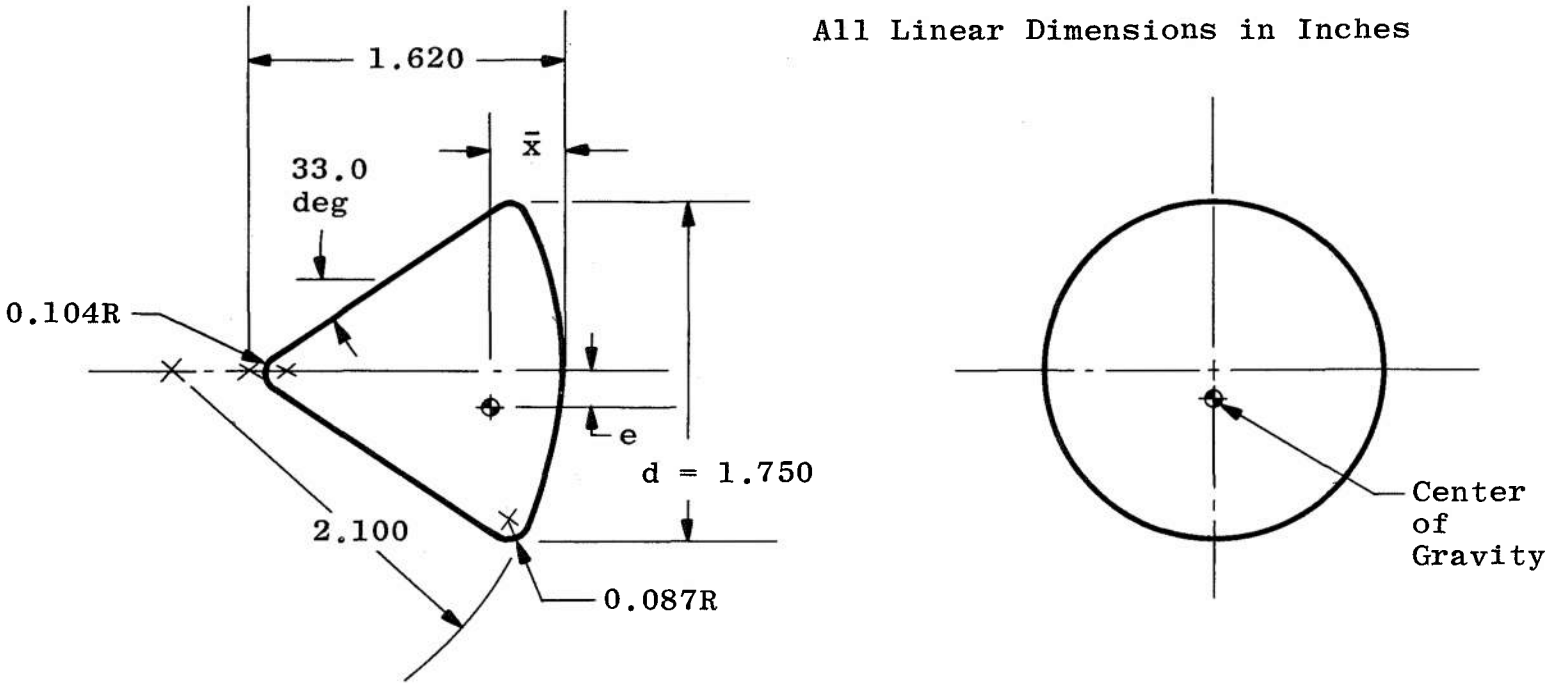

Fig. 2 Nominal External Model Dimensions

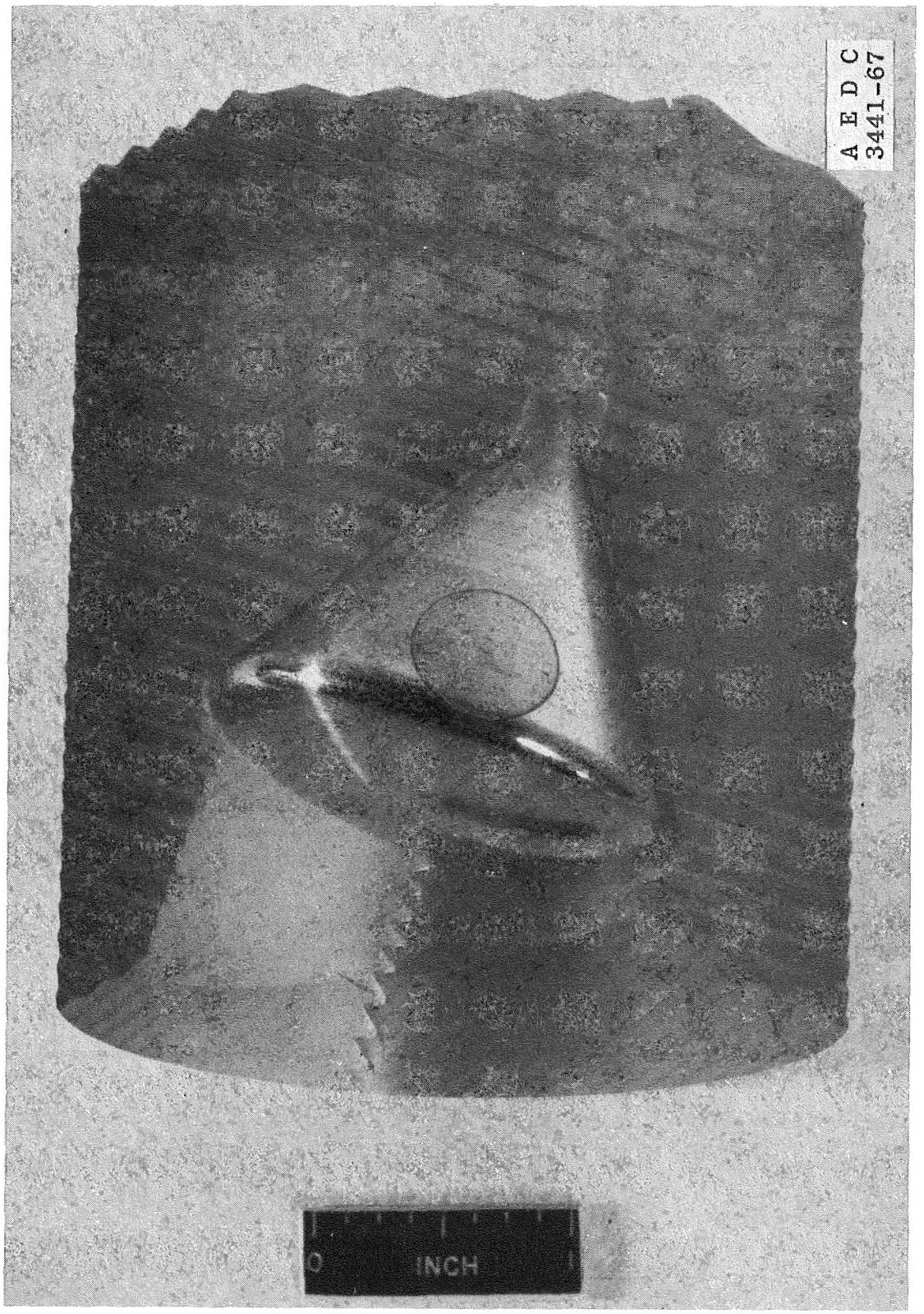

Fig. 3 Photograph of Model and Partial Sabot

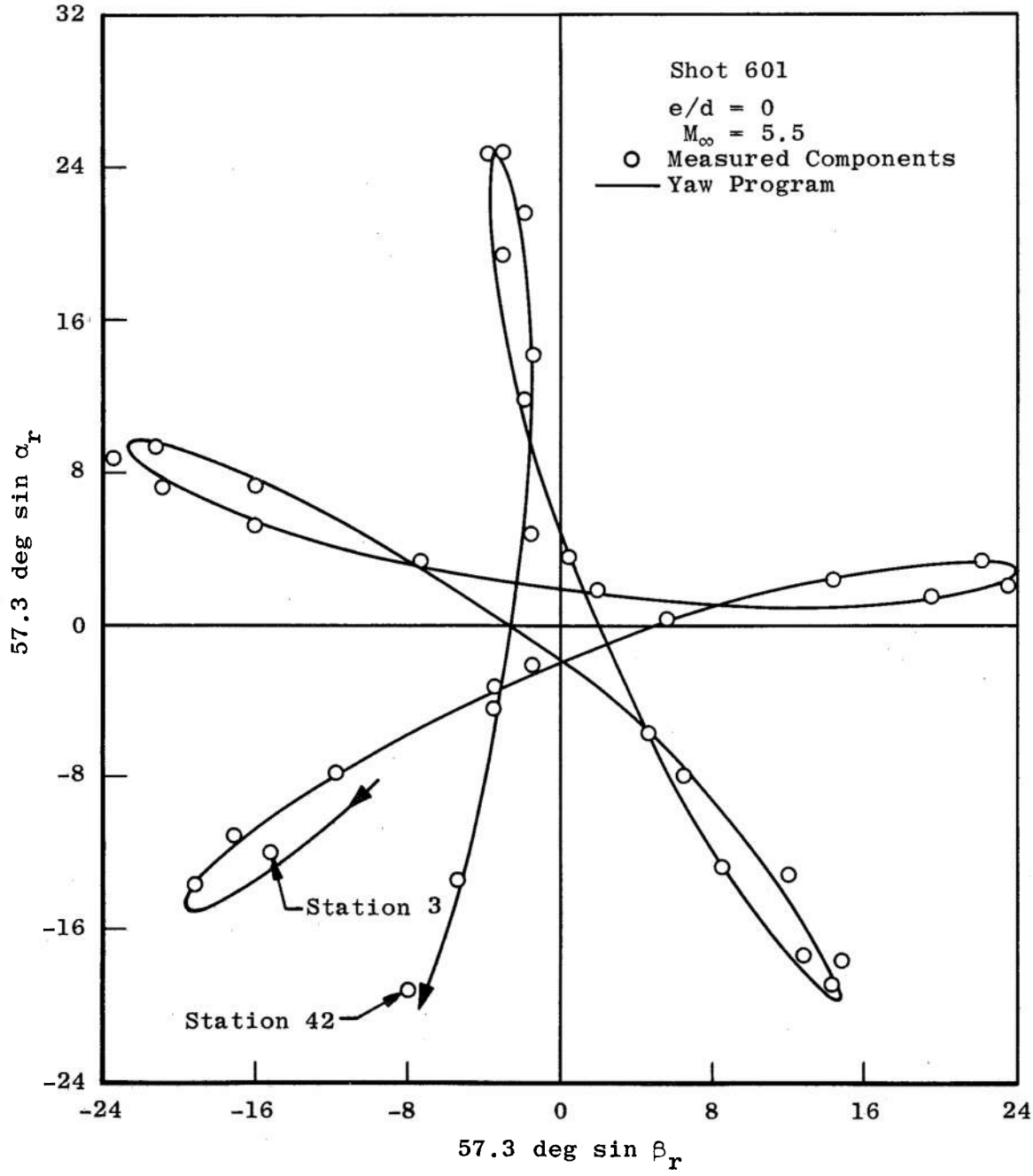

a. Symmetrical Model

Fig. 4 Typicol Yawing Motions ond Curve Fits

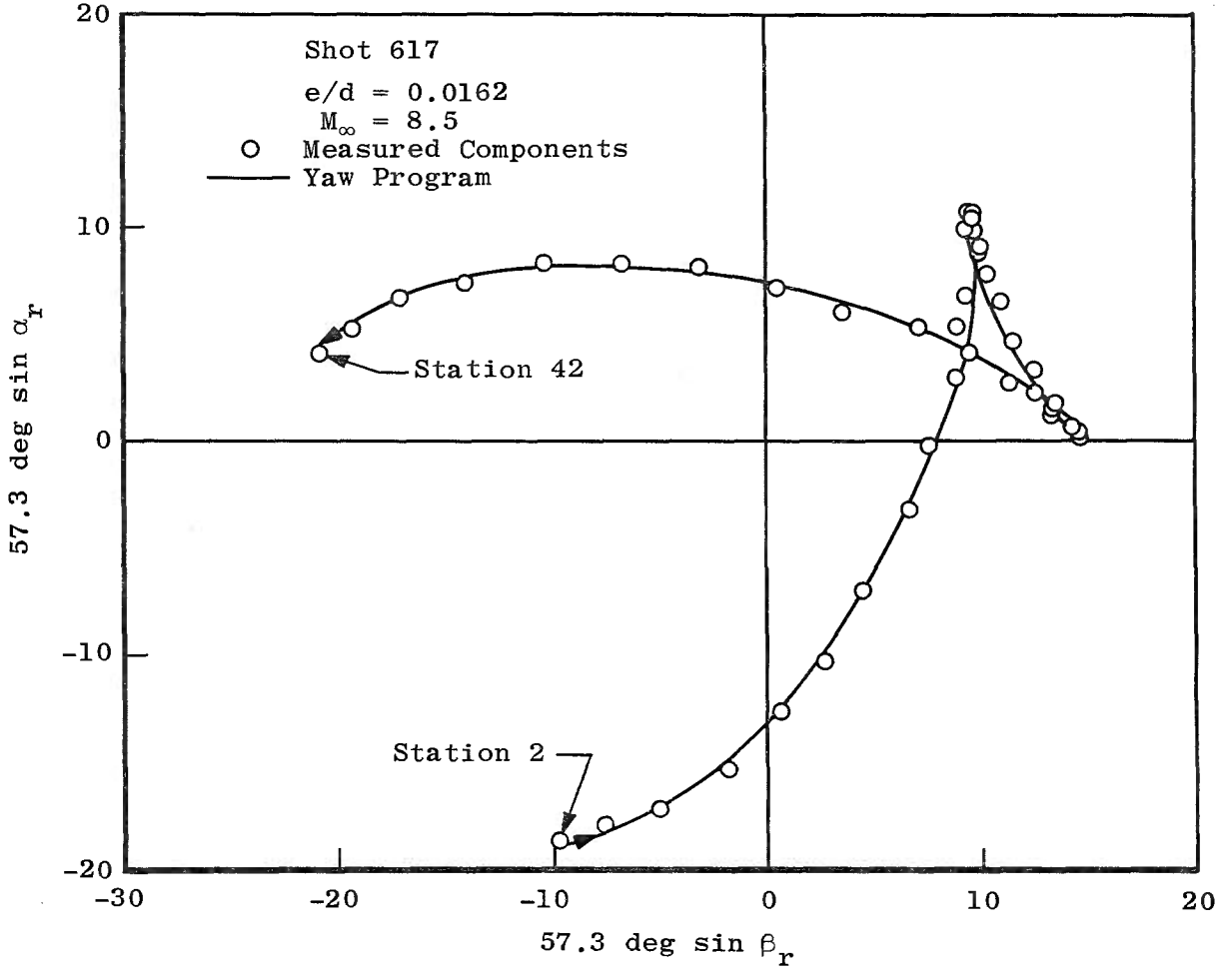

b. Half-Offset Model

Fig. 4 Continued

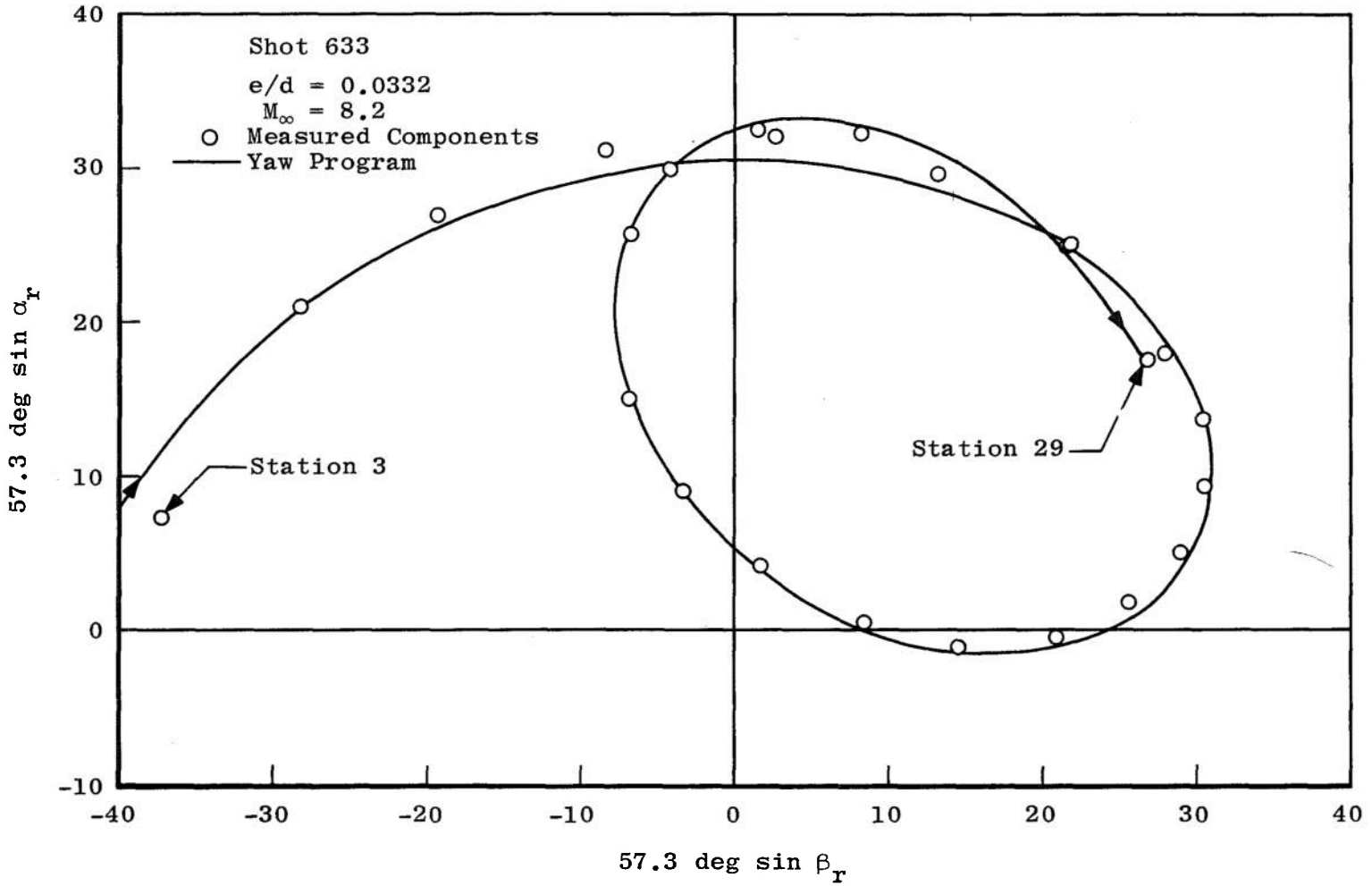

c. Full-Offset Model

Fig. 4 Concluded

Symbol	Source	M_∞	$Re_{2d} \times 10^{-4}$
○	Range Data, Rolling Trim	8.5	1.2 → 3.9
△	Range Data, Rolling Trim	6	2.4 → 7.2
●	Range Data, Adjusted to Zero Roll Rate	8.5	1.2 → 3.9
□	Wind Tunnel Data, Ref. 1	7.9	11.2
◇	Wind Tunnel Data, Ref. 1	8.0	3.8 → 19.2

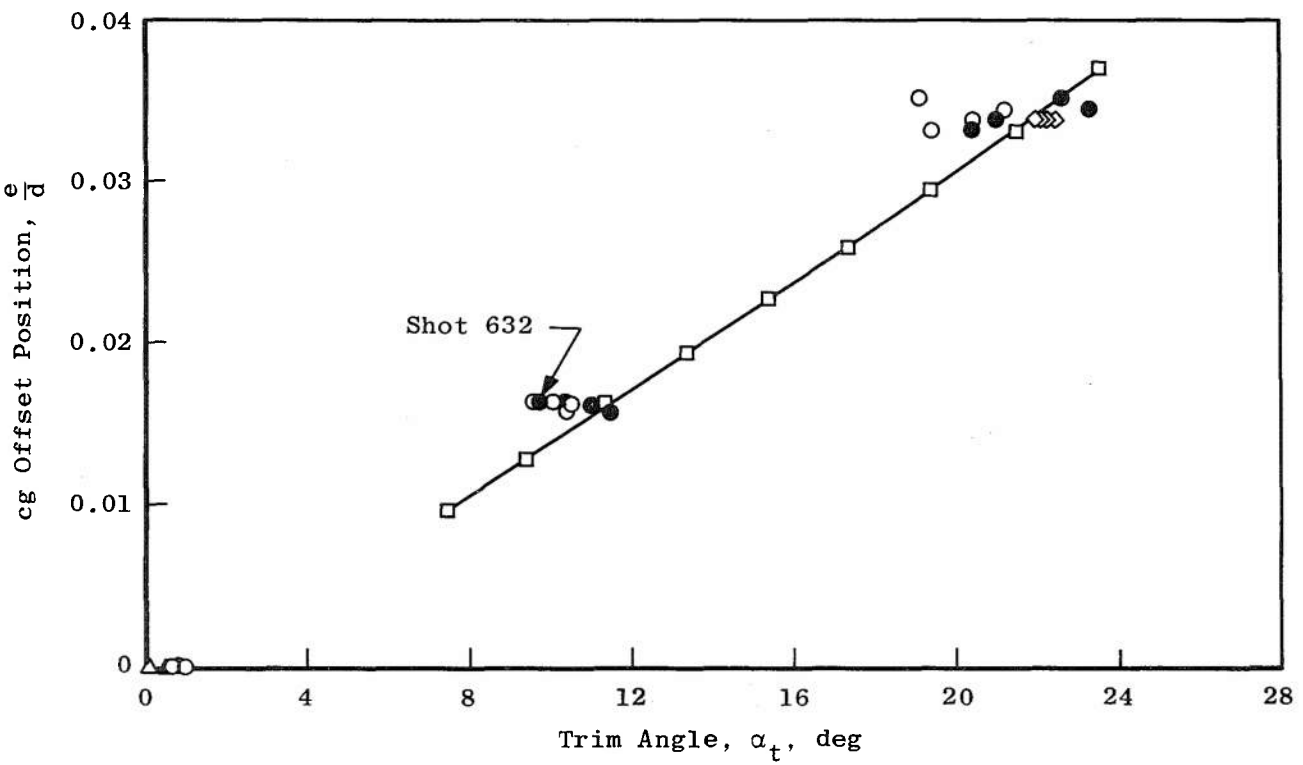

a. Linear Analysis

Fig. 5 Trim Angle as a Function of Center-of-Gravity Offset Position

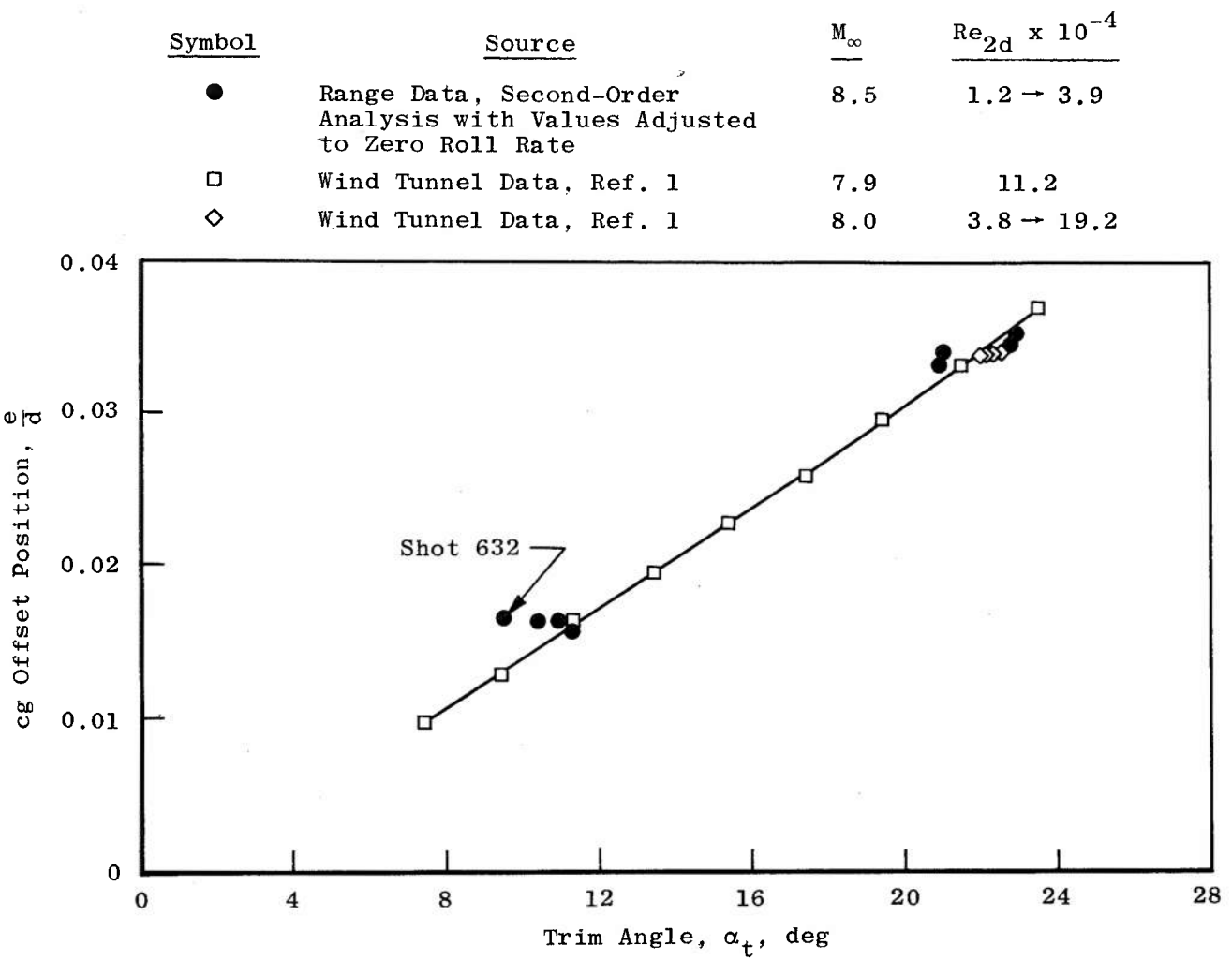

b. Second-Order Analysis

Fig. 5 Concluded

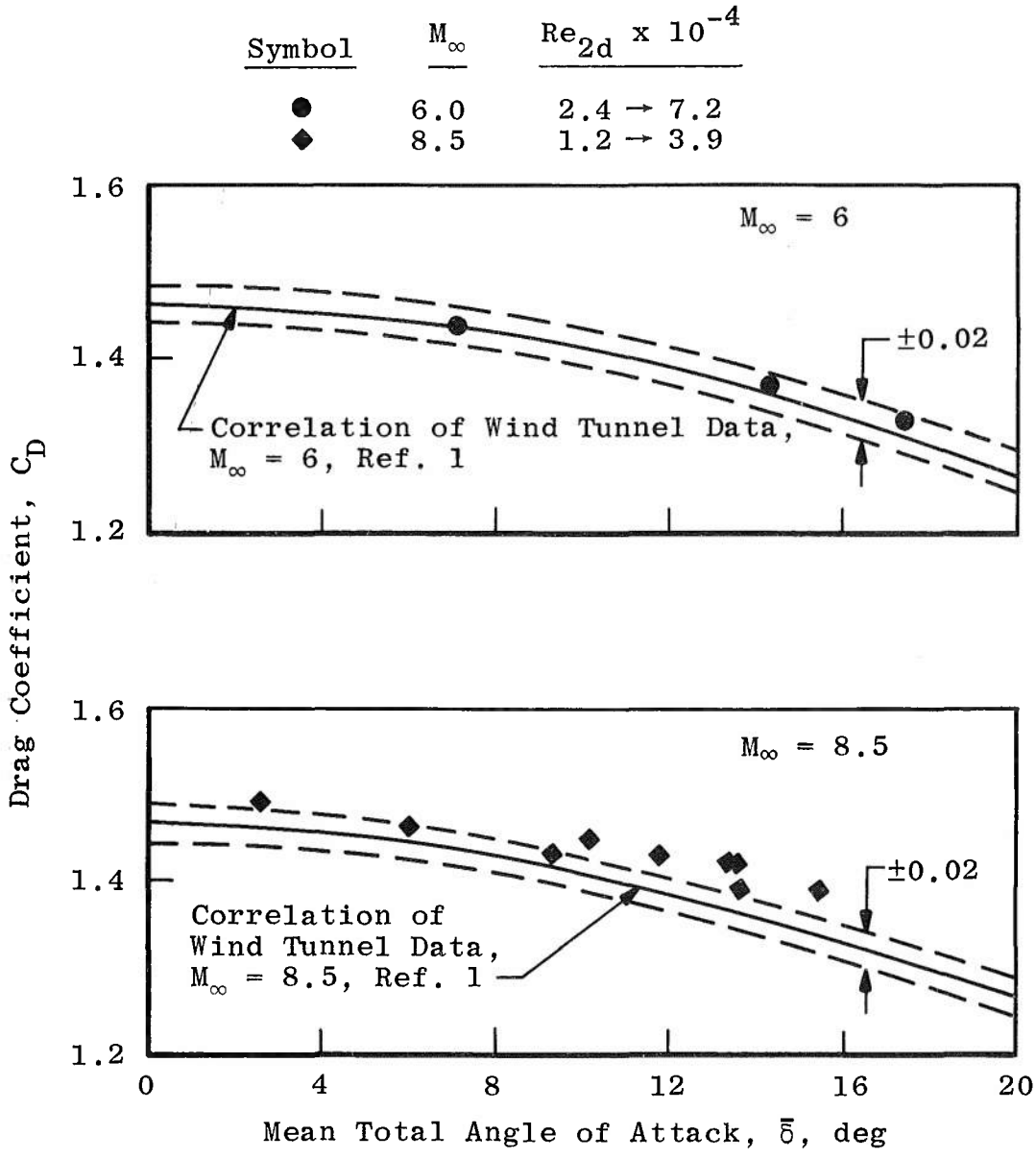

Fig. 6 Drag Coefficient as a Function of Mean Total Angle of Attack

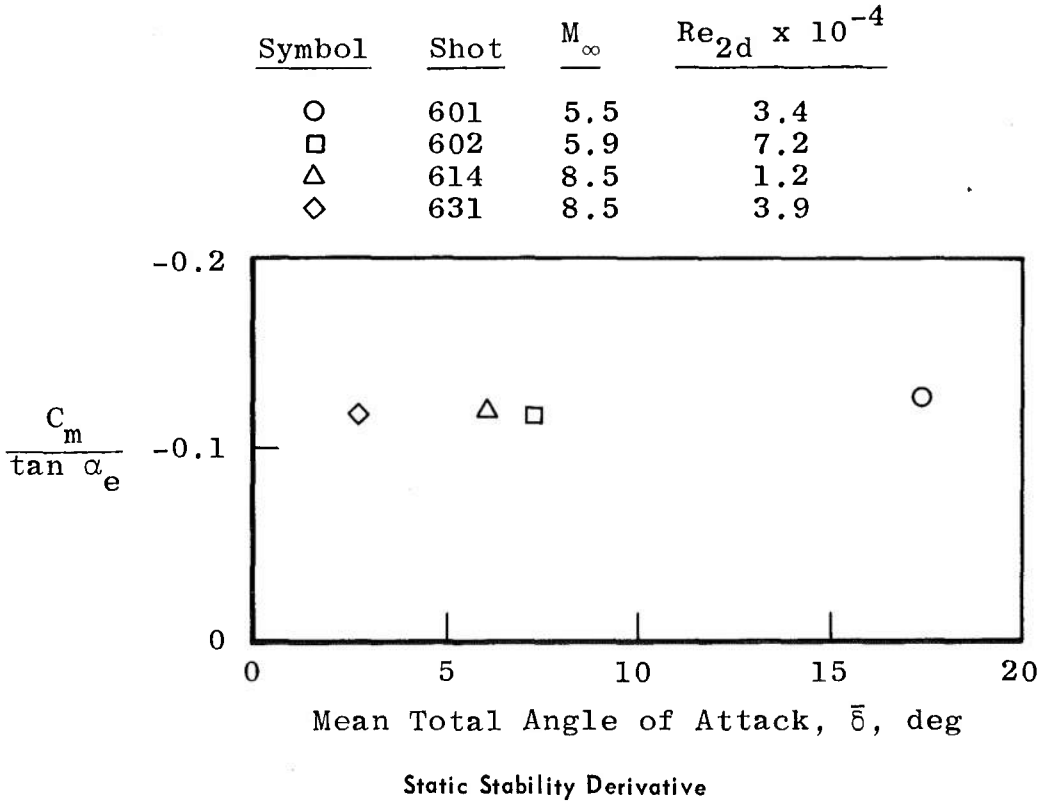

Static Stability Derivative

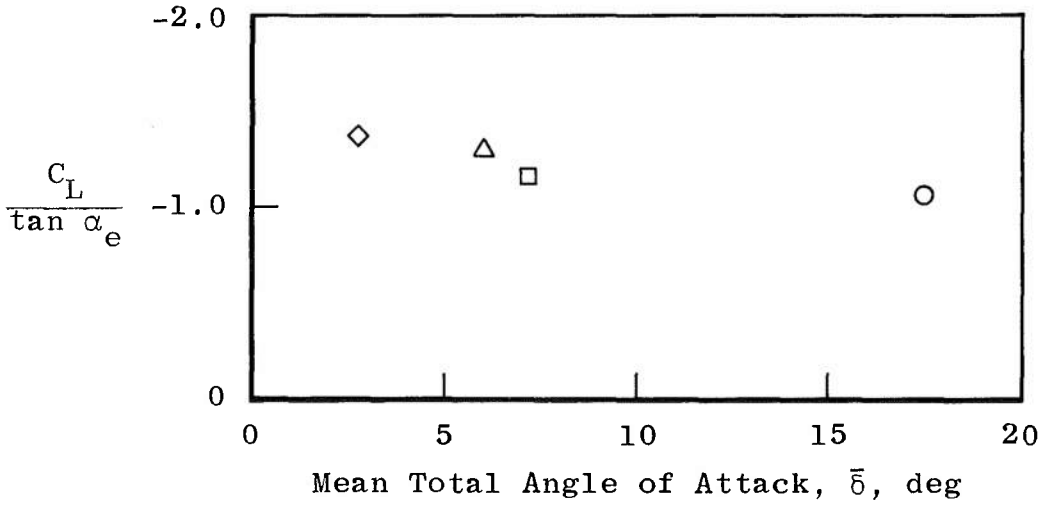

b. Slope of Lift Curve

Fig. 7 Effective Static Stability Derivative and Slope of Lift Curve

Wind Tunnel Data			
Symbol	Source	M_∞	$Re_{2d} \times 10^{-4}$
▽	Ref. 1	7.9	11.2
○	Ref. 1	7.9	3.8

Range Data			
Shot	M_∞	$Re_{2d} \times 10^{-4}$	$\bar{\delta}$, deg
614	8.5	1.2	6.0
631	8.5	3.9	2.6

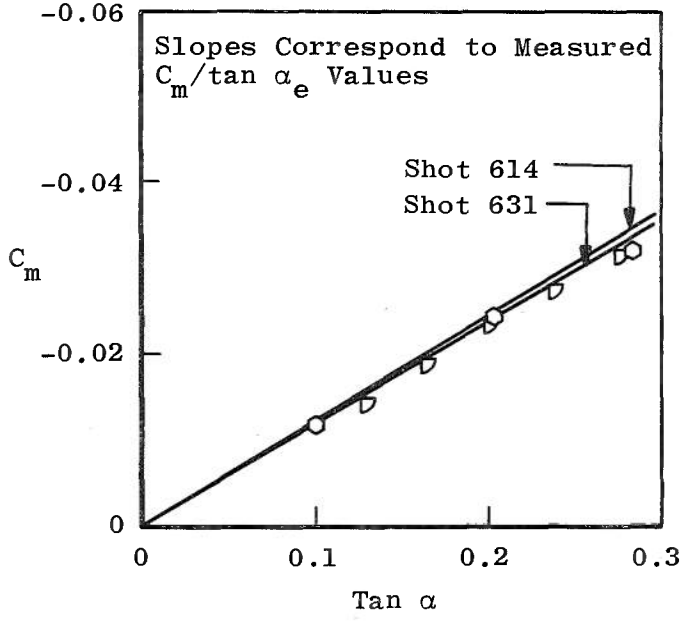

a. Pitching-Moment Coefficient

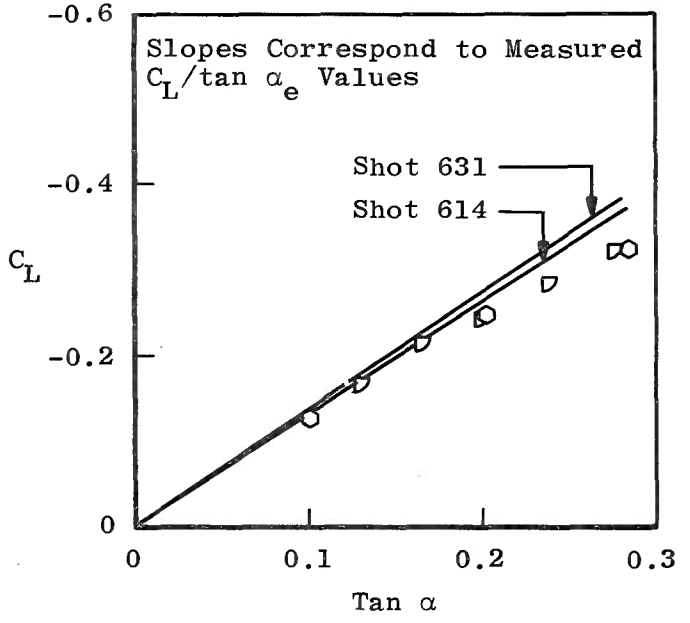

b. Lift Coefficient

Fig. 8 Comparison of Range and Wind Tunnel Stability Data at M ≈ 8

TABLE I

PHYSICAL CHARACTERISTICS OF MODELS

Shot	d, in.	$\bar{x}/d$	e/d	$m \times 10^2$, slugs	$I_x \times 10^5$, slug-ft^2	$I_y \times 10^5$, slug-ft^2	$I_z \times 10^5$, slug-ft^2
600	1.750	0.242	0.0002	1.282	2.387	1.751	
601	1.747	0.244	0.0005	1.279	2.387	1.764	
602	1.749	0.242	0.0004	1.279	2.388	1.757	
614	1.749	0.274	0.0002	1.361	2.384	1.961	
631	1.751	0.272	0.0001	1.357	2.380	1.963	
615	1.750	0.273	0.0157	1.279	2.252	1.801	1.934
617	1.751	0.274	0.0162	1.284	2.226	1.803	1.935
619	1.751	0.274	0.0163	1.286	2.237	1.807	1.935
632	1.749	0.274	0.0164	1.286	2.243	1.800	1.951
616	1.750	0.270	0.0344	1.364	2.423	1.992	1.964
618	1.751	0.270	0.0351	1.360	2.434	1.989	1.965
620	1.751	0.271	0.0339	1.358	2.407	1.985	1.963
633	1.752	0.275	0.0332	1.345	2.416	1.974	1.950

TABLE II
TEST CONDITIONS AND AERODYNAMIC DATA

Shot Number	Range Pressure, mm Hg	M_∞	$Re_{\infty d} \times 10^{-4}$	$Re_{2d} \times 10^{-4}$	P, deg/ft	$\bar{\delta}$, deg	Drag Program	Swerve Program	Yaw Program			Second-Order Analysis	
							C_D	$\frac{C_L}{\tan \alpha_e}$	α_t, deg	α_{t_o}, deg	$\frac{C_m}{\tan \alpha_e}$	α_t, deg	α_{t_o}, deg
Symmetrical													
600	10.3	5.93	8.00	2.38		14.3	1.37		0.1				
601	15.2	5.47	10.80	3.35		17.4	1.33	-1.06	0.1		-0.126		
602	31.3	5.88	24.10	7.15		7.1	1.44	-1.17	0.5		-0.119		
614	4.7	8.52	5.19	1.23	0.53	6.0	1.46	-1.31	0.7		-0.120		
631	15.6	8.47	17.20	3.94	0.11	2.6	1.49	-1.38	1.0		-0.118		
Half Offset													
615	4.9	8.57	5.50	1.30	0.44	10.2	1.45[1]		10.4	11.5		10.4	11.3
615						9.3	1.43[2]						
617	4.7	8.46	5.20	1.23	0.30	13.4	1.42[3]		10.5	11.0		10.6	11.0
617						13.7	1.39[2]						
619	8.4	8.16	8.96	2.11	0.30	24.1			10.1	10.4		10.2	10.4
632	14.2	8.66	16.00	3.59	0.14	13.5	1.42		9.7	9.7		9.5	9.5
Full Offset													
616	4.8	8.37	5.24	1.25	0.34	15.5	1.39		21.2	23.3		21.0	22.8
618	4.7	8.72	5.37	1.24	0.47	11.8	1.43		19.1	22.6		19.8	22.9
620	8.3	8.38	9.09	2.12	0.32	22.6			20.4	21.0		20.4	21.0
633	8.1	8.19	8.62	2.03	-0.28	30.2			19.4	20.4		20.2	20.9

[1]Determined Over the Interval from 0 to 600 ft

[2]Determined Over the Interval from 320 to 600 ft

[3]Determined Over the Interval from 0 to 840 ft

APPENDIX III
BASIC DATA REDUCTION PROCEDURES FOR RANGE TESTS

This appendix describes the conventional techniques used in reducing aerodynamic data from measurements of the model motion during the test flight of the model. Three different types of data reduction programs are involved:

1. A yaw program for determining the static stability parameter, the damping parameter, and the trim angle from the yawing motion of the model.
2. A swerve program for determining the lift-force derivative from the transverse motion of the model cg.
3. A drag program for determining the drag coefficient from the longitudinal motion of the model.

1. YAW PROGRAM

In Ref. 2, Murphy derived a differential equation for the motion of an axisymmetric model in free flight. This equation, referenced to a right-hand, nonrolling axis system, can be written as

$$\xi'' + \left(H_1 - \frac{\gamma'}{\gamma} - i P_1\right)\xi' - (M + i P_1 T)\xi = 0 \qquad \text{(III-1)}$$

in which

$$\xi = \frac{V_1}{V_\infty} + i\frac{W_1}{V_\infty} = \sin\beta_r + i \sin\alpha_r$$

Additional quantities are:

$$H_1 = \left(\frac{\rho A}{2M}\right)\left[\frac{C_L}{\tan\alpha_e} - C_D - k_t^2\left(C_{m_q} + \gamma C_{m_{\dot\alpha}}\right)\right]$$

$$M = \left(\frac{\rho A d}{2I_y}\right)\left[\frac{C_m}{\tan\alpha_e} - \left(\frac{\rho A}{2m}\right)\gamma C'_{L_\alpha}\right]$$

$$T = \left(\frac{\rho A}{2m}\right)\left[\frac{C_L}{\tan\alpha_e} + \gamma k_a^{-2} C_{m_{p_\alpha}}\right]$$

$$P_1 = \left(\frac{I_x}{I_y}\right)P$$

$$\alpha_e = \sin^{-1}|\xi|$$

$$\gamma = \cos\alpha_e$$

$$()' = \frac{d()}{dx}$$

(See Fig. IV-7 and the list of symbols for definitions of the above parameters.)

It is to be noted that the lift and moment coefficients appear in the terms

$$\frac{C_L}{\tan \alpha_e} \quad \text{and} \quad \frac{C_m}{\tan \alpha_e}$$

rather than the more conventional forms

$$\gamma C_{L_\alpha} \text{ and } \gamma C_{m_\alpha}$$

This has been done to make clear that the equation is valid even for large angles. It should also be pointed out that the coefficients C_L and C_m are to be evaluated at the total angle of attack, α_e, and need not be linear functions of angle of attack.

Equation (III-1) is valid for a symmetrical vehicle, and in the computer program the usual assumptions that $\gamma' = C'_{L_\alpha} = 0$ were made and the coefficients were assumed constants. Therefore, the program yields effective mean values of the quantity $C_m/\tan \alpha_e$.

Small configurational asymmetries can be handled approximately by introducing an exponential forcing function into the right-hand side of Eq. (III-1) (Ref. 2), and the solution of the differential equation with this additional trim term can be written as

$$\xi = A_1 \exp(\mu_1 + i\,\phi_1')x + A_2 \exp(\mu_2 + i\,\phi_2')x + A_3 \exp(i\,Px) \qquad \text{(III-2)}$$

The use of Eq. (III-2) requires assumptions of linear variation of aerodynamic forces and moments with $\tan \alpha_e$, equal static stability derivatives in pitch and yaw, small configurational asymmetries, and a constant roll rate. Further, for small amplitude motion the assumption that $\gamma = 1$ can be made.

In a linear analysis of a model's angular motion, Eq. (III-2) is fitted to the measured components of the complex yaw angle, ξ, as functions of the distance traveled, x, using a differential corrections procedure (Ref. 3). There are ten equation constants to be determined in fitting Eq. (III-2). The A's, in general, are complex numbers; however, P can be expressed as a function of ϕ'_1 and ϕ'_2. The quantities A_1 and A_2 depend on the initial launch disturbances encountered by the model, but the magnitude of A_3 is related to the rolling-model trim angle of attack by the relation

$$\sin \alpha_t = A_3$$

The trim angle of a free-flight model corresponding to zero roll (see Ref. 2) can be expressed as

$$\alpha_{t_o} = \alpha_t \left[1 + P^2 \frac{(1 - I_x/I_y)}{\phi_1' \phi_2'} \right] \qquad \text{(III-3)}$$

Zero damping, assumed in this expression, is a quite valid assumption.

The stability parameters can be expressed in terms of the determined equation constants by the following relationships:

$$\frac{C_m}{\tan \alpha_e} = \left(\frac{2I_y}{\rho A d}\right) \phi_1' \phi_2' \tag{III-4}$$

$$D = \frac{2m}{\rho A}(\mu_1 + \mu_2) \tag{III-5}$$

in which

$$D = C_D - \frac{C_L}{\tan \alpha_e} + k_t^{-2}\left(C_{m_q} + C_{m_{\dot{\alpha}}}\right)$$

It is apparent that if Eq. (III-2) (linear) is applied to a model that has nonlinear characteristics the reduced stability parameters are mean values corresponding to the motion interval involved.

2. SWERVE PROGRAM

The lift-curve slope is obtained from an analysis of the transverse motion of the model (Ref. 2). The differential equation defining the transverse motion, referenced to a right-hand, range-fixed coordinate system with the x-axis along the range axis, can be written as

$$y'' + iz'' = -\frac{\rho A}{2m}\left[\left(\frac{C_L}{\tan \alpha_e} + iPd\, C_{N_{p_\alpha}}\right)\xi_1 + (-C_{y_o} - iC_{z_o}) \exp(iPx)\right] \tag{III-6}$$

in which

$$\xi_1 = \frac{V_1}{U_1} + i\frac{W_1}{U_1}$$

Assuming that the coefficients are constant, Eq. (III-6) may be integrated twice to yield

$$y + iz = (y_o + iz_o) + (y_o' + iz_o')x - \left(\frac{C_L}{\tan \alpha_e} + iPdC_{N_{p_\alpha}}\right)(G + iH) + (C_{y_o} + iC_{z_o})(I + iJ) \tag{III-7}$$

where

$$G + iH = \frac{\rho A}{2m}\int_0^x \int_0^{x_2} \xi_1 \, dx_1 \, dx_2$$

$$I + iJ = \frac{\rho A}{2mP^2}[(1 - \cos Px) + i(Px - \sin Px)]$$

and an o subscript indicates the initial value. Equation (III-7) is fitted to the measured (y + iz) values by a least-squares curve-fitting procedure to obtain a value for $C_L/\tan \alpha_e$.

3. DRAG PROGRAM

The drag coefficient, C_D, was obtained from the relation

$$C_D = -\left(\frac{2m}{\rho A \overline{V}_\infty}\right) \frac{dV}{dx} \qquad \text{(III-8)}$$

in which dV/dx is the mean slope of the curve of model velocity as a function of distance traveled, and $\overline{V}_\infty$ is the mean model velocity during the interval of the flight trajectory being examined. Equation (III-8) is based on the assumption that C_D is constant during the flight interval of concern and has been found to provide quite adequate results when the total velocity drop during the flight interval is less than about 4 percent of the initial velocity. Since a model's angular amplitude, in general, will vary along the trajectory, the drag coefficient obtained by this procedure corresponds to the mean total angle of attack experienced by the model. This mean angle of attack is defined by the relation

$$\overline{\delta^2} = \frac{1}{L_2 - L_1} \int_{L_1}^{L_2} \left[\sin^{-1} \sqrt{|\xi|^2}\right]^2 dx = \frac{1}{L_2 - L_1} \int_{L_1}^{L_2} \alpha_e^2 \, dx \qquad \text{(III-9)}$$

where $L_2 - L_1$ is the length of the flight interval over which C_D is computed.

APPENDIX IV
SECOND-ORDER THEORY

The comparison of trim angles based on wind tunnel data with those determined from the range data by the yaw program (Appendix III) shows a scatter of approximately ±1.5 deg. The second-order treatment of this appendix was undertaken in an attempt to reduce this scatter by accounting for certain known small effects with the aid of available wind tunnel data. The result leads to only a minor reduction in the scatter. Nevertheless, the complete treatment is included because it points out some interesting peculiarities in the moment curve of the particular shape being studied, and it presents in a specific example an extension of the basic work of Murphy (Ref. 2) to the case of a vehicle with asymmetries which are not necessarily small.

DYNAMIC EQUATIONS

The yaw program (Appendix III) is written in terms of the range axis system, using the angles α_r and β_r. This is the most advantageous system for a completely symmetrical vehicle. During the tests covered in this report, conditions were encountered for which the assumption of symmetry was not justified, so that it was necessary to obtain results with respect to a body-fixed axis system.

The following equations for a body-fixed axis system with products of inertia equal to zero are from Etkin (Ref. 4).

$$M = I_y \frac{dQ}{dt} - FI_y\ PR = C_m\ qAd \qquad \text{(IV-1)}$$

$$N = I_z \frac{dR}{dt} + GI_z\ PQ = C_n\ qAd \qquad \text{(IV-2)}$$

in which

$$F = \frac{I_z - I_x}{I_y} \qquad \text{(IV-3)}$$

$$G = \frac{I_y - I_x}{I_z} \qquad \text{(IV-4)}$$

The body-fixed axis system is shown in Fig. IV-1. The angular velocities are in units of radians per second.

The relationships among the velocity components and the angular velocity components are also obtained from Etkin.

$$\frac{dV}{dt} + RU - PW = Y/m + g \cos\theta \sin\Phi \tag{IV-5}$$

$$\frac{dW}{dt} + PV - QU = Z/m + g \cos\theta \cos\Phi \tag{IV-6}$$

in which Y and Z are the aerodynamic forces, and θ and Φ are the elevation and roll angle, respectively, of the axis system relative to an inertial system. The approximation is now made that the right-hand sides of these two expressions may be neglected. Neglecting the gravitational terms can be easily justified. The aerodynamic force terms, if included, would appear as damping terms in the final equations. Provision for damping will be added at a later stage in the development. Neglecting the damping terms at this point is equivalent to neglecting the differences in the damped and undamped natural frequencies, which can be justified on the basis of the small damping associated with the particular configuration being considered.

The velocity components V and W are now eliminated by using the angles of attack, α, and sideslip, β, defined by (Fig. IV-2)

$$\left.\begin{aligned} U &= V_\infty \cos\alpha \cos\beta \\ V &= V_\infty \cos\alpha \sin\beta \\ W &= V_\infty \sin\alpha \\ V_\infty &= \sqrt{U^2 + V^2 + W^2} \end{aligned}\right\} \tag{IV-7}$$

Including only terms up to second-order in α and β simplifies these to

$$\begin{aligned} U &= V_\infty [1 - (\alpha^2 + \beta^2)/2] \\ V &= V_\infty \beta \\ W &= V_\infty \alpha \end{aligned}$$

These results may now be used in Eqs. (IV-5) and (IV-6). In doing so, P is considered a quantity of zero order, and Q and R are considered quantities of first order. At the same time, the conversion is made from time, t, to distance, x, as the independent variable, by using

$$\frac{dx}{dt} = V_\infty$$

The angular velocities are then measured in radians per foot. The results, correct to the second order, are

$$\frac{d\beta}{dx} + R - P\alpha = 0 \tag{IV-8}$$

$$\frac{d\alpha}{dx} + P\beta - Q = 0 \tag{IV-9}$$

These are now used in Eqs. (IV-1) and (IV-2) to give

$$\frac{d^2\alpha}{dx^2} - FP^2\alpha + P(1 + F)\frac{d\beta}{dx} = \frac{C_m\, qAd}{V_\infty^2\, I_y} \qquad \text{(IV-10)}$$

$$-P(1 + G)\frac{d\alpha}{dx} + \frac{d^2\beta}{dx^2} - GP^2\beta = -\frac{C_n\, qAd}{V_\infty^2\, I_z} \qquad \text{(IV-11)}$$

Further derivation depends upon determining the functional dependence of the moment coefficients on the angles α and β.

MOMENT COEFFICIENTS

Figure IV-3 gives wind tunnel data for the pitching-moment and axial-force coefficients as a function of angle of attack from Ref. 1. These may be represented by*

$$C_{m_1} = -0.00220\alpha + 0.0000085\,\alpha^2 \qquad \text{(IV-12)}$$

$$C_A = 1.465 - 0.000339\,\alpha^2 \qquad \text{(IV-13)}$$

The pitching moment C_{m_1} is taken about the point on the axis of the vehicle at which the plane perpendicular to the axis which contains the offset cg intersects the axis (Fig. IV-4). The pitching moment about the offset cg is

$$C_m = C_A\frac{e}{d} + C_{m_1} \qquad \text{(IV-14)}$$

Let

$$\frac{e}{d} = 0.03384\,P_o$$

in which P_o represents the fraction of offset (i. e., $P_o = 1$ corresponds to the full-offset case). Then

$$C_m = (1.465 - 0.000339\,\alpha^2)\,(0.03384\,P_o) - 0.00220\,\alpha + 0.0000085\,\alpha^2 \qquad \text{(IV-15)}$$

---

*The data given in Fig. IV-3 are more accurately represented by

$$C_{m_1} = -0.00208\alpha + 0.0000050\,\alpha^2$$

for the smaller angles. The representation given by Eq. (IV-12) was used in the second-order data reduction program because it represents the data better at the large angles. The effects of the slight differences are negligible for the development in this appendix.

From this relation, the trim condition can be determined. The following results are obtained:

P_o	α_t, deg
0	0
0.5	11.4
1.0	21.9

The representation for the pitching moment given by Eq. (IV-15) is valid only if the velocity vector lies in the x-y plane. If the velocity vector is outside the x-y plane (i. e., the vehicle is at a sideslip), then more care must be taken in choosing the representation.

The location of the cg is unimportant for determining the magnitude of the aerodynamic moment and C_A. Therefore, the magnitudes of these quantities are determined by the total angle of attack, α_e, which is defined as the angle between the x-axis, or the axis of symmetry, and the velocity vector, measured in the plane containing the two. Therefore, if

$$\alpha_e = \sqrt{\alpha^2 + \beta^2} \tag{IV-16}$$

$$C_A = 1.465 - 0.000339\,\alpha_e^2 \tag{IV-17}$$

and

$$C_{m_{11}} = -0.00220\,\alpha_e + 0.0000085\,\alpha_e^2 \tag{IV-18}$$

The projections of the total moment coefficient on the appropriate axis then give the pitching- and yawing-moment coefficients relative to the axis system fixed in the offset cg (Fig. IV-4)

$$C_{m_1} = C_{m_{11}}\,\alpha/\alpha_e \tag{IV-19}$$

$$C_n = C_{m_{11}}\,\beta/\alpha_e \tag{IV-20}$$

Therefore,

$$C_m = -0.00220\,\alpha + C_2\,\alpha\alpha_e + 0.0496\,P_o - C_1\,\alpha_e^2 \tag{IV-21}$$

$$C_n = 0.00220\,\beta - C_2\beta\alpha_e \tag{IV-22}$$

in which

$$C_1 = 0.0000115\,P_o \tag{IV-23}$$

$$C_2 = 0.0000085 \tag{IV-24}$$

Figure IV-5 shows the resulting pitching moment as a function of α and β, and shows that a vehicle undergoing a yawing oscillation will trim at a lower value of α than one that is not yawing.

FURTHER DEVELOPMENT OF EQUATIONS

The expressions for the pitching and yawing moments are now introduced into Eqs. (IV-10) and (IV-11). The damping terms will be added later.

$$\frac{d^2\alpha}{dx} + \left(0.00220\,\frac{qAd}{V_\infty^2\, I_y} - FP^2\right)\alpha + P(1 + F)\,\frac{d\beta}{dx}$$

$$= \frac{qAd}{V_\infty^2 I_y}\,(C_2\alpha\alpha_e + 0.0496\,P_o - C_1\,\alpha_e^2) \qquad \text{(IV-25)}$$

$$-P(1 + G)\,\frac{d\alpha}{dx} + \frac{d^2\beta}{dx^2} + \left(0.00220\,\frac{qAd}{V_\infty^2\, I_z} - GP^2\right)\beta = \frac{qAd}{V_\infty^2\, I_z}\,C_2\beta\alpha_e \qquad \text{(IV-26)}$$

The following development has two objectives:

1. The equations are to be written with all linear terms on the left side and the nonlinear terms on the right-hand side.
2. The numbers 0.00220 and 0.0496 P_o appearing in the moment expressions will be eliminated in favor of the natural frequencies and the trim angle, which are the quantities that may be determined from the range tests.

The nonlinear quantities C_1 and C_2 will be retained at the values given by the wind tunnel tests, since it is thought that it is not possible to evaluate these small parameters from the range data.

From Eqs. (IV-25) and (IV-26), the steady-state condition is

$$\beta = 0$$

$$\alpha = \alpha_e = \alpha_t \qquad \text{(IV-27)}$$

so

$$\left(0.00220\,\frac{qAd}{V_\infty^2\, I_y} - FP^2\right)\alpha_t = \frac{qAd}{V_\infty^2\, I_y}\,[(C_2 - C_1)\,\alpha_t^2 + 0.0496\,P_o] \qquad \text{(IV-28)}$$

At this value of α, we find from Eq. (IV-21)

$$C_{m_{\alpha o}} = -0.00220 + 2(C_2 - C_1)\,\alpha_t \qquad \text{(IV-29)}$$

It is therefore convenient to define the oscillating frequency for small oscillations by

$$\omega_\alpha^2 = -\frac{C_{m_{\alpha_o}}\, qAd}{V_\infty^2\, I_y} \qquad \text{(IV-30)}$$

$$= [0.00220 - 2(C_2 - C_1).\alpha_t]\,\frac{qAd}{V_\infty^2\, I_y}$$

The effect of the roll rate on the static stiffness is apparent from Eq. (IV-28). In order to compare with wind tunnel data, the trim angle for zero roll rate must be determined, whereas the range data "solve" Eq. (IV-28) with non-zero roll rate. Since the correction for roll rate is small, the second-order terms of Eq. (IV-28) (those involving $C_2 - C_1$) may be neglected in evaluating the correction. With this assumption, the trim angle without roll, α_{t_o}, is related to that with roll, α_t, by

$$\alpha_{t_o} = \alpha_t \left[1 - F \left(\frac{P}{\omega_\alpha}\right)^2\right] \qquad \text{(IV-31)}$$

The parameters α_t, P, and ω_α are to be determined from the range data by the technique described later.

In order to eliminate the parameters obtained from the wind tunnel data, the term 0.0496 P_o in Eq. (IV-25) is eliminated by using Eq. (IV-28). The term involving the parameter 0.00220 is eliminated by using Eq. (IV-30). In addition, the following substitutions are made:

$$\alpha = \alpha_t + \alpha_1 \qquad \text{(IV-32)}$$

$$K_1 = C_1/|C_{m_{\alpha_o}}| \qquad \text{(IV-33)}$$

$$K_2 = C_2/|C_{m_{\alpha_o}}| \qquad \text{(IV-34)}$$

Equation (IV-25) then becomes

$$\frac{d^2\alpha_1}{dx^2} + (\omega_\alpha^2 - FP^2)\alpha_1 + P(1 + F)\frac{d\beta}{dx} = \omega_\alpha^2 [\alpha_t\alpha_e + \alpha_1\alpha_e - \alpha_t^2 - 2\alpha_t\alpha_1) - K_1(\alpha_1^2 + \beta^2)] \qquad \text{(IV-35)}$$

Similarly, for the yaw equation, let

$$C_{n_{\beta_o}} = 0.00220 - C_2\alpha_t \qquad \text{(IV-36)}$$

$$\omega_\beta^2 = \frac{C_{n_{\beta_o}} qAd}{V_\infty^2 I_z} \qquad \text{(IV-37)}$$

$$K_3 = C_2/C_{n_{\beta_o}} \qquad \text{(IV-38)}$$

Equation (IV-26) then becomes

$$-P(1 + G)\frac{d\alpha_1}{dx^2} + \frac{d^2\beta}{dx^2} + (\omega^2_\beta - GP^2)\beta = \omega^2_\beta K_3(\alpha_e - \alpha_t) \qquad \text{(IV-39)}$$

One further simplification is introduced. In obtaining the second-order solution, the term α_e is troublesome. Therefore, an approximation will be made to the value of this term. In general,

$$\alpha_e = \sqrt{\alpha_t^2 + 2\alpha_t\alpha_1 + \alpha_1^2 + \beta^2} \qquad \text{(IV-40)}$$

Assume that α_t^2 is the dominant term, and the remaining terms are small. Then

$$\alpha_e \approx \alpha_t + \alpha_1 + \frac{\alpha_1^2 + \beta^2}{2\alpha_t} \tag{IV-41}$$

This is used in Eqs. (IV-35) and (IV-39) to give

$$\frac{d^2 \alpha_1}{dx^2} + \omega_A^2 \alpha_1 + P(1 + F) \frac{d\beta}{dx} = \omega_\alpha^2 [F_1 \alpha_1^2 + F_2 \beta^2] \tag{IV-42}$$

and

$$- P(1 + G) \frac{d\alpha_1}{dx} + \frac{d^2\beta}{dx^2} \omega_B^2 \beta = \omega_\beta^2 K_3 \alpha_1 \beta \tag{IV-43}$$

in which

$$\begin{aligned} F_1 &= 1.5 K_2 - K_1 \\ F_2 &= 0.5 K_2 - K_1 \end{aligned} \tag{IV-44}$$

$$\begin{aligned} \omega_A^2 &= \omega_\alpha^2 - FP^2 \\ \omega_B^2 &= \omega_\beta^2 - GP^2 \end{aligned} \tag{IV-45}$$

In obtaining these results, third-order terms in α_1 and β have been neglected.

LINEAR SOLUTIONS

The linear solution to Eqs. (IV-42) and (IV-43) is obtained by neglecting the right-hand sides. The resulting equations to be solved are

$$\frac{d^2 \alpha_1}{dx^2} + \omega_A^2 \alpha_1 + P(1 + F) \frac{d\beta}{dx} = 0 \tag{IV-46}$$

$$- P(1 + G) \frac{d\alpha_1}{dx} + \frac{d^2\beta}{dx^2} + \omega_B^2 \beta = 0 \tag{IV-47}$$

The characteristic equation is given by

$$\begin{vmatrix} s^2 + \omega_A^2 & P(1 + F)s \\ -P(1 + G)s & s^2 + \omega_B^2 \end{vmatrix} = 0 \tag{IV-48}$$

or

$$s^4 + [\omega_B^2 + \omega_B^2 + (1 + F)(1 + G)P^2] s^2 + \omega_A^2 \omega_B^2 = 0$$

This may be factored to

$$(s^2 + \omega_1^2)(s^2 + \omega_2^2) = 0$$

The relations among ω_1, ω_2, ω_A, and ω_B are found to be

$$\begin{aligned}
\omega_1 &= 0.5\left[\sqrt{(\omega_A + \omega_B)^2 + Z_1} + S\sqrt{(\omega_A - \omega_B)^2 + Z_1}\right] \\
\omega_2 &= 0.5\left[\sqrt{(\omega_A + \omega_B)^2 + Z_1} - S\sqrt{(\omega_A - \omega_B)^2 + Z_1}\right] \\
\omega_A &= 0.5\left[\sqrt{(\omega_1 + \omega_2)^2 - Z_1} + S\sqrt{(\omega_1 - \omega_2)^2 - Z_1}\right] \\
\omega_B &= 0.5\left[\sqrt{(\omega_1 + \omega_2)^2 - Z_1} - S\sqrt{(\omega_1 - \omega_2)^2 - Z_1}\right]
\end{aligned} \tag{IV-49}$$

in which

$$Z_1 = (1 + F)(1 + G)P^2 \tag{IV-50}$$

$$\begin{aligned}
S &= +1 \quad \omega_A > \omega_\beta;\ \omega_1 > \omega_2 \\
&\quad -1 \quad \omega_A < \omega_\beta;\ \omega_1 < \omega_2
\end{aligned} \tag{IV-51}$$

The solution to the equations may be written

$$\alpha_1 = D_\alpha \sin(\omega_1 x + \delta_\alpha) + T_2 D_\beta \cos(\omega_2 x + \delta_\beta) \tag{IV-52}$$

$$\beta = D_\beta \sin(\omega_2 x + \delta_\beta) - T_1 D_\alpha \cos(\omega_1 x + \delta_\alpha) \tag{IV-53}$$

The solution has been set up so that as the roll rate P goes to zero, the solution with frequency ω_1 becomes the oscillation in α. The parameters T_1 and T_2 are given by

$$T_1 = \frac{\omega_1^2 - \omega_A^2}{\omega_1 P(1 + F)} = \frac{\omega_B\omega_1 - \omega_A\omega_2}{\omega_B P(1 + F)} \tag{IV-54}$$

$$T_2 = \frac{\omega_2^2 - \omega_B^2}{\omega_2 P(1 + G)} = \frac{\omega_A\omega_2 - \omega_B\omega_1}{\omega_A P(1 + G)} = -\frac{1 + F}{1 + G}\frac{\omega_B}{\omega_A}T_1 \tag{IV-55}$$

It should be noted that for a completely symmetrical vehicle, the above results yield

$$\begin{aligned}
\omega_1 - \omega_2 &= S(1 + F)P \\
T_1 &= S \\
T_2 &= -S
\end{aligned}$$

PARTIAL SECOND-ORDER SOLUTION

One method of obtaining a solution to Eqs. (IV-42) and (IV-43) is to use the perturbation method (Ref. 5). The technique is based upon the assumption that the nonlinear terms are small, so that an approximate

evaluation of these terms can be used. For the particular problem under consideration, this involves using the solutions to the linear case as given by Eqs. (IV-52) and (IV-53) in the right-hand sides of Eqs. (IV-42) and (IV-43), and obtaining new solutions for α_1 and β. The solution will then appear as the linear solution plus additional second-order terms.

Upon combining Eqs. (IV-42) and (IV-43) for α_1 and β, there is obtained

$$\frac{d^4 \alpha_1}{dx^2} + (\omega_1^2 + \omega_2^2) \frac{d^2 \alpha_1}{dx^2} + \omega_1^2 \omega_2^2 \alpha_1 = \omega_\alpha^2 \left(\frac{d^2}{dx^2} + \omega^2_B\right) (F_1 \alpha_1^2 + F_2 \beta^2)\Big|_0$$

$$- \omega_\beta^2 K_3 P(1 + F) \frac{d}{dx} (\alpha_1 \beta)\Big|_0 \qquad \text{(IV-56)}$$

$$\frac{d^4 \beta}{dx^4} + (\omega_1^2 + \omega_2^2) \frac{d^2 \beta}{dx^2} + \omega_1^2 \omega_2^2 \beta = \omega_\beta^2 K_3 \left(\frac{d^2}{dx^2} + \omega^2_A\right) (\alpha_1 \beta)\Big|_0$$

$$+ P(1 + G) \omega_\alpha^2 \frac{d}{dx} (F_1 \alpha_1^2 + F_2 \beta^2)\Big|_0 \qquad \text{(IV-57)}$$

with the understanding that the expressions for α_1 and β given by Eqs. (IV-52) and (IV-53) are used in the right-hand sides of these equations.

It should be obvious that the resulting solution is quite lengthy. It was decided to limit the solution to the two largest terms, the constant term, and the terms involving sines and cosines with frequency $\omega_1 - \omega_2$. There are also terms involving sines and cosines with frequencies $2\omega_1$, $2\omega_2$, and $\omega_1 + \omega_2$. The coefficients of these terms are small because of the higher frequencies, and furthermore, the data from the range seldom covered more than one cycle of frequency ω_1 or ω_2, so that these terms have not been included in the remaining development.

With these simplifications, the solution becomes

$$\alpha = \alpha_0 + \frac{\omega_\alpha^2}{2\omega_A^2} [(F_1 + T_1^2 F_2) D_\alpha^2 + (F_2 + T_2^2 F_1) D_\beta^2] + D_\alpha \sin(\omega_1 x + \delta_\alpha)$$

$$+ T_2 D_\beta \cos(\omega_2 x + \delta_\beta) + D_\alpha D_\beta [\omega_\alpha^2 (F_1 T_1 + F_2 T_1) (\omega_B^2 - (\omega_1 - \omega_2)^2)$$

$$+ 0.5 K_3 P (1 + F) \omega_\beta^2 (\omega_1 - \omega_2)(1 - T_1 T_2)] \frac{\sin(\omega_1 x + \delta_\alpha - \omega_2 x - \delta_\beta}{\omega_1 \omega_2 (2\omega_1 - \omega_2)(2\omega_2 - \omega_1)} \qquad \text{(IV-58)}$$

$$\beta = D_\beta \sin(\omega_2 x + \delta_\beta) - T_1 D_\alpha \cos(\omega_1 x + \delta_\alpha) + D_\alpha D_\beta [\omega_\beta^2 K_3 (1 - T_1 T_2)$$

$$(\omega_A^2 - (\omega_1 - \omega_2)^2)/2 + \omega_\alpha^2 (\omega_1 - \omega_2) P(1 + G)(F_1 T_2 + F_2 T_1)]$$

$$\frac{\cos(\omega_1 x + \delta_\alpha - \omega_2 x - \delta_\beta)}{\omega_1 \omega_2 (2\omega_1 - \omega_2)(2\omega_2 - \omega_1)} \qquad \text{(IV-59)}$$

These are the equations that were fitted to the data.

RELATIONSHIPS INVOLVING RANGE ANGLES AND BODY-FIXED ANGLES

The data from the range consist of values of the elevation angle, α_r, and the yaw angle, β_r, at various stations along the range. Relationships must be found between these angles and angles α and β appearing in the equations derived in this appendix. Referring to Fig. IV-6, two axes systems are shown, an xyz system, fixed in the model (as shown in Fig. IV-1), and an $x_r y_r z_r$ system fixed in the range, with x_r directed along the range axis, z_r vertically downward, and y_r horizontal and forming a right-hand system. The vector $\vec{a}$ is the vector from the center of mass perpendicular to the axis of the vehicle (Fig. IV-1). The orientation of the xyz system relative to the $x_r y_r z_r$ system is specified by three angles defined as follows:

1. Beginning with the $x_r y_r z_r$ system, rotate about the x_r axis through the roll angle, ϕ, to the $x_r y_i z_i$ axis system, which contains the center of mass and the vector $\vec{a}$.
2. Rotate about the y_i axis through the angle of attack, α, to the $x_i y_i z$ axis, so that the vector $\vec{a}$ lies along the z axis.
3. Rotate about the z axis through the sideslip angle, β, to the xyz axis system, so that the x axis is parallel to the axis of the vehicle.

The unit vector $\vec{i}$ along the x axis of the vehicle can be related to the unit vectors $\vec{i}_r$, $\vec{j}_r$, and $\vec{k}_r$ of the $x_r y_r z_r$ system. The result is

$$\vec{i} = \cos\alpha \cos\beta \vec{i}_r + (\sin\alpha \cos\beta \sin\phi - \sin\beta \cos\phi)\vec{j}_r - (\sin\alpha \cos\beta \cos\phi + \sin\beta \sin\phi)\vec{k}_r \qquad \text{(IV-60)}$$

The range angles are the elevation angle, α_r, and the yaw angle, β_r. These are defined with respect to an $x_1 y_1 z_1$ coordinate system, which has its x_1 axis along the x axis of the vehicle, and the y_1 axis horizontal. This is therefore a nonrolling body axes system. The orientation of this axis system relative to the range axis system is specified by two angles, β_1 and θ_1, defined as follows (Fig. IV-7).

1. Rotate about the z_r axis through an angle β_1 to the $x_j y_1 z_r$ axis system, so that the x axis lies in the $x_j z_r$ plane.
2. Rotate about the y_1 axis through an angle θ, to the $x_1 y_1 z_1$ axis, so that the x_1 axis coincides with the x axis.

For this transformation

$$\vec{i} = \cos\beta_1 \cos\theta_1 \vec{i}_r - \sin\beta_1 \cos\theta_1 \vec{j}_r - \sin\theta_1 \vec{k}_r \qquad \text{(IV-61)}$$

Equating the corresponding coefficients of Eqs. (IV-60) and (IV-61) gives

$$\left.\begin{aligned} \cos\beta_1 \cos\theta_1 &= \cos\alpha \cos\beta \\ \sin\beta_1 \cos\theta_1 &= -\sin\alpha \cos\beta \sin\phi + \sin\beta \cos\phi \\ \sin\theta_1 &= \sin\alpha \cos\beta \cos\phi + \sin\beta \sin\phi \end{aligned}\right\} \quad \text{(IV-62)}$$

Therefore,

$$\tan\beta_1 = -\tan\alpha \sin\phi + \tan\beta \cos\phi/\cos\alpha \quad \text{(IV-63)}$$

$$\tan\theta_1 = \cos\beta_1 [\tan\alpha \cos\phi + \tan\beta \sin\phi/\cos\alpha] \quad \text{(IV-64)}$$

The angles α_r and β_r are defined such that (Fig. IV-7)

$$\left.\begin{aligned} V &= V_\infty \sin\beta_r \\ W &= V_\infty \sin\alpha_r \end{aligned}\right\} \quad \text{(IV-65)}$$

Therefore,

$$\left.\begin{aligned} \sin\beta_r &= \sin\beta_1 \\ \sin\alpha_r &= \cos\beta_1 \sin\theta_1 \end{aligned}\right\} \quad \text{(IV-66)}$$

For small angles in θ_1 and β_1, these simplify to

$$\left.\begin{aligned} \alpha_r &= \cos\phi\ \alpha + \sin\phi\ \beta \\ \beta_r &= -\sin\phi\ \alpha + \cos\phi\ \beta \end{aligned}\right\} \quad \text{(IV-67)}$$

Both the nonlinear relations (Eqs. (IV-63), (IV-64), and (IV-66)) and the linear relations (Eq. (IV-67)) have been used in the data reduction program, and differences were noted for only one run.

The roll angle ϕ can be expanded by

$$\phi = Px + \phi_o \quad \text{(IV-68)}$$

SOLUTION PROCEDURE

The solutions given by Eqs. (IV-58) and (IV-59) give the angle of attack, α_1, and the sideslip angle, β, in terms of the distance x and the parameters ω_α, ω_β, P, α_o, D_α, D_β, δ_α, and $\delta\beta$. In addition a damping term of the form e^{-DX} was applied to the first-order oscillatory terms. The same value of D was used for both modes, since the damping was quite small.

The solution procedure consisted of using the method of differential corrections (Ref. 3) to determine the parameters ω_α, ω_β, P, α_o, D_α, $D\beta$, δ_α, $\delta\beta$, ϕ_o, and D to minimize the sum of the squares of the differences between the calculated values of α_r and β_r and the experimental values.

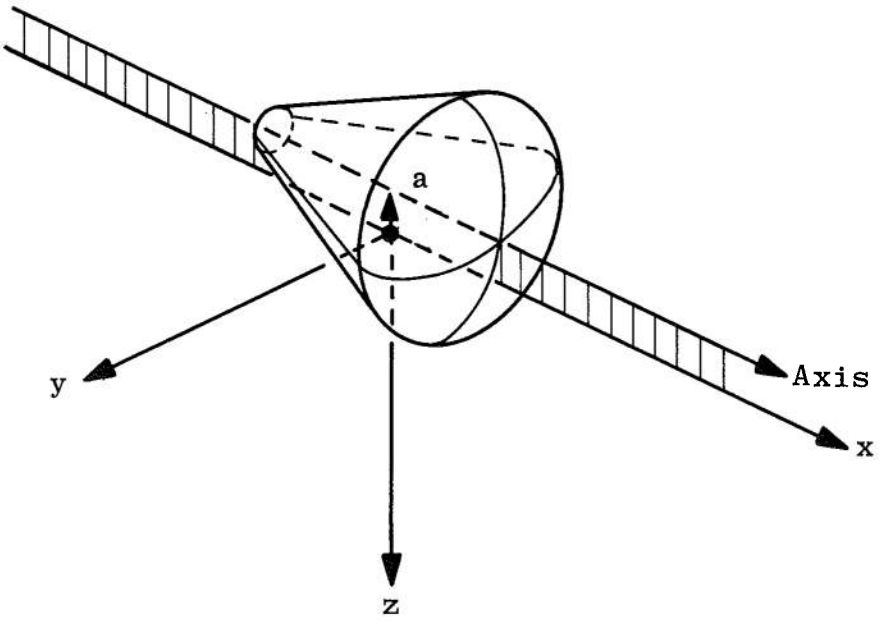

Fig. IV-1 Body-Fixed Axis System

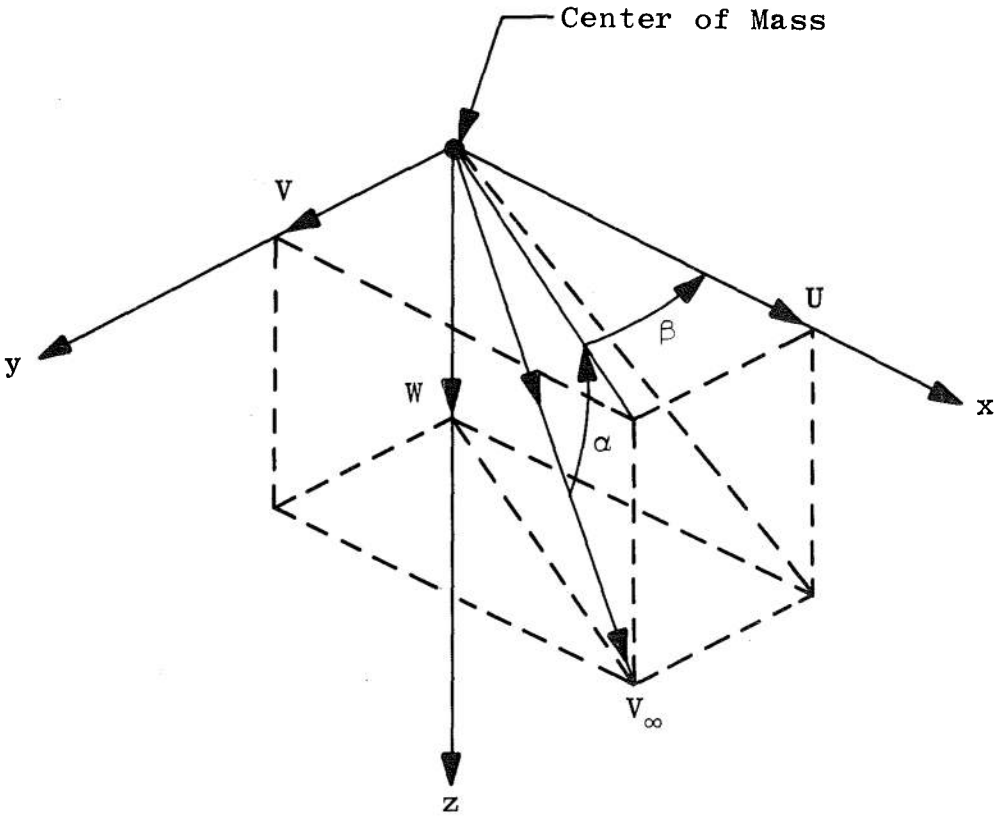

Fig. IV-2 Definitions of Angles α and β

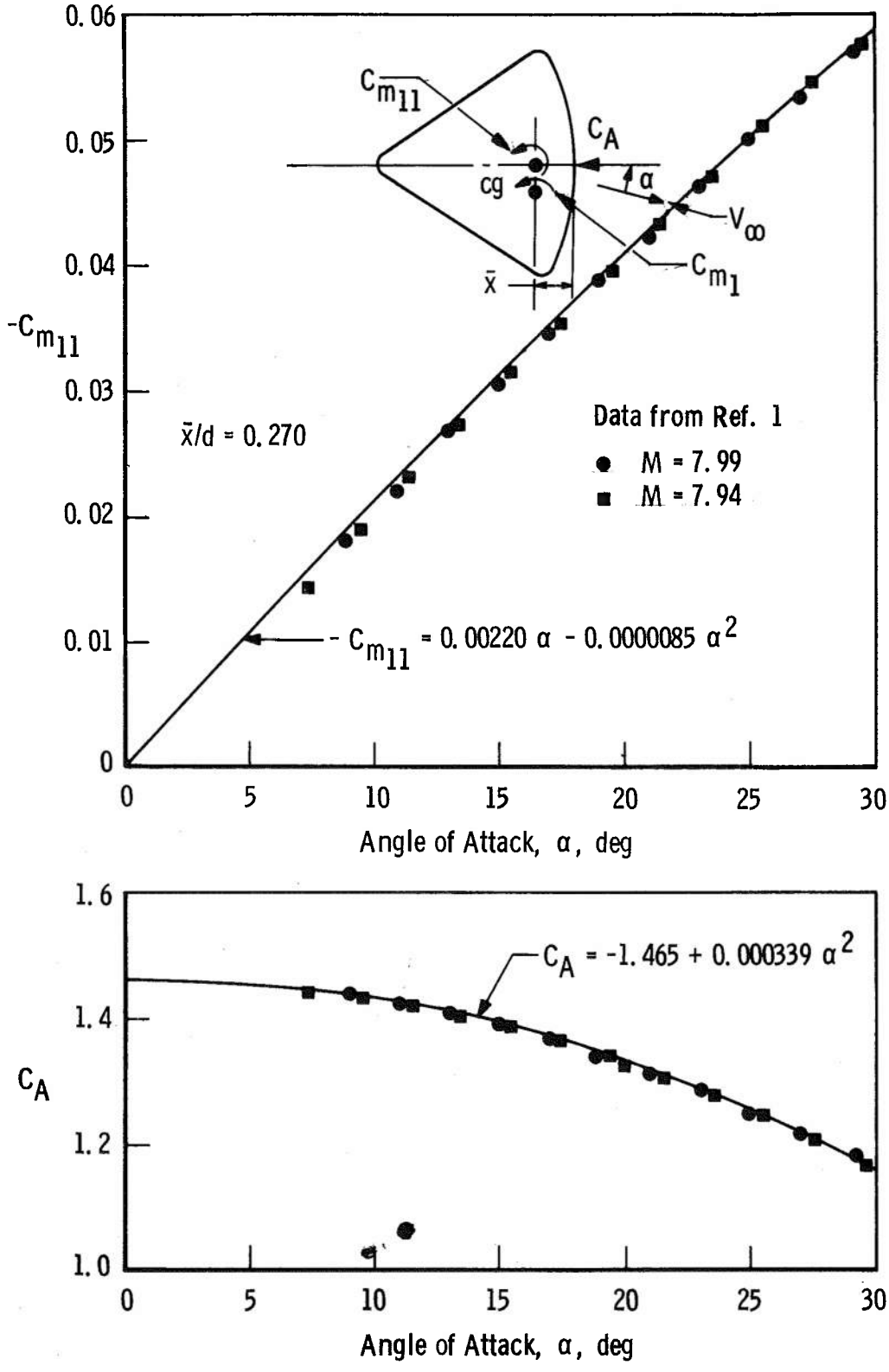

Fig. IV-3 Wind Tunnel Data for Moment and Axial Force

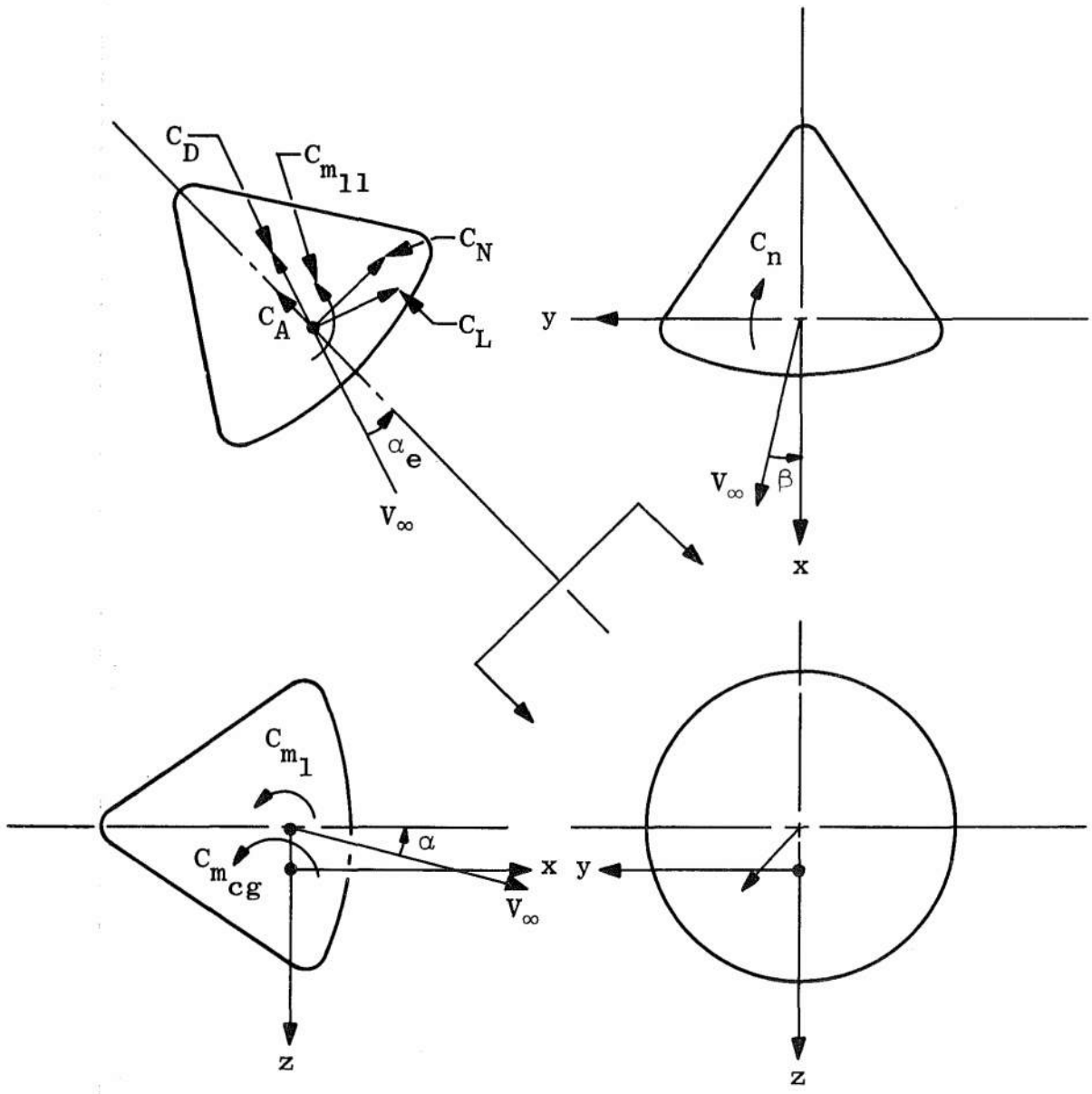

Fig. IV-4 Projection of Moments

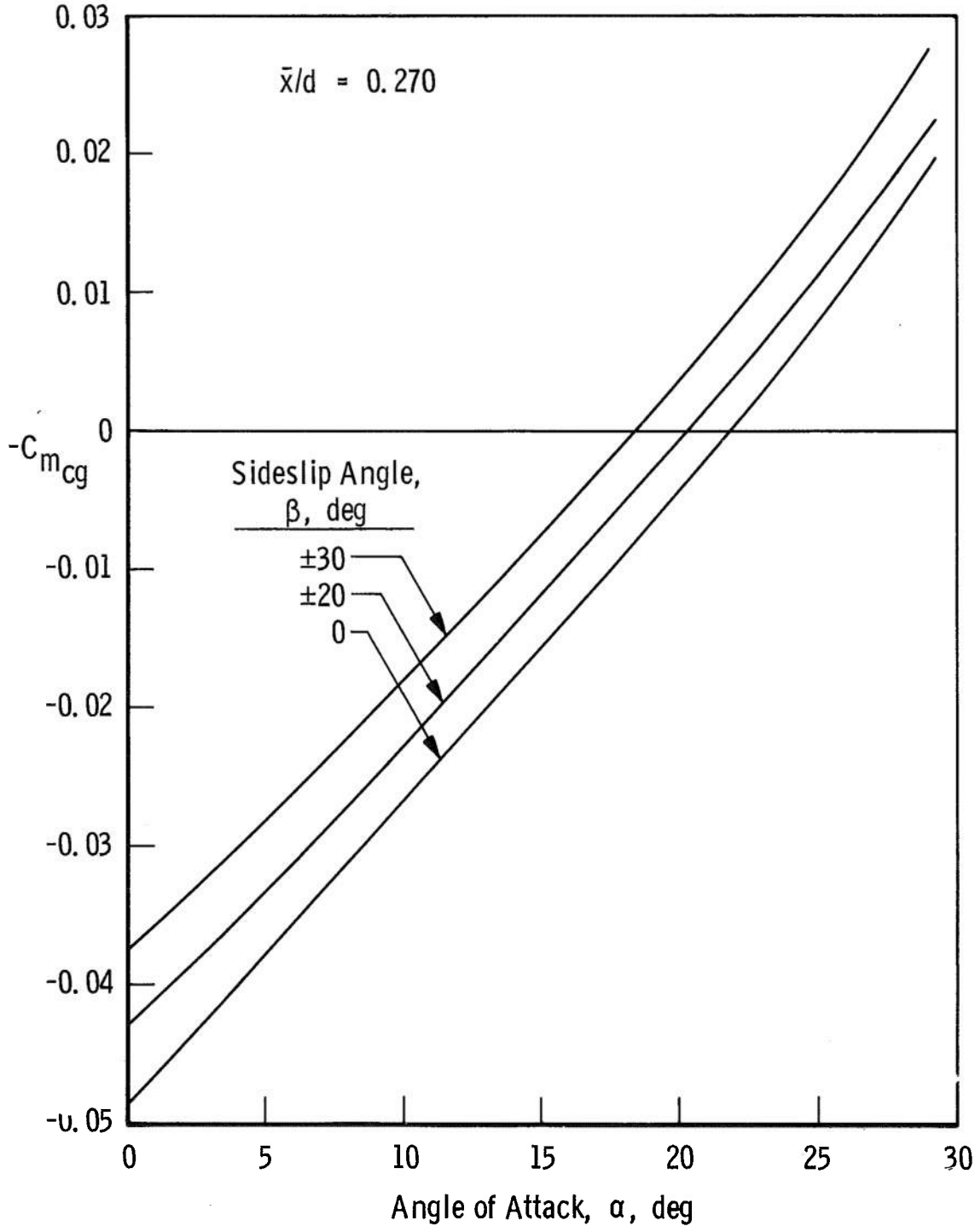

Fig. IV-5 Pitching-Moment Coefficient about Full-Offset Center of Gravity

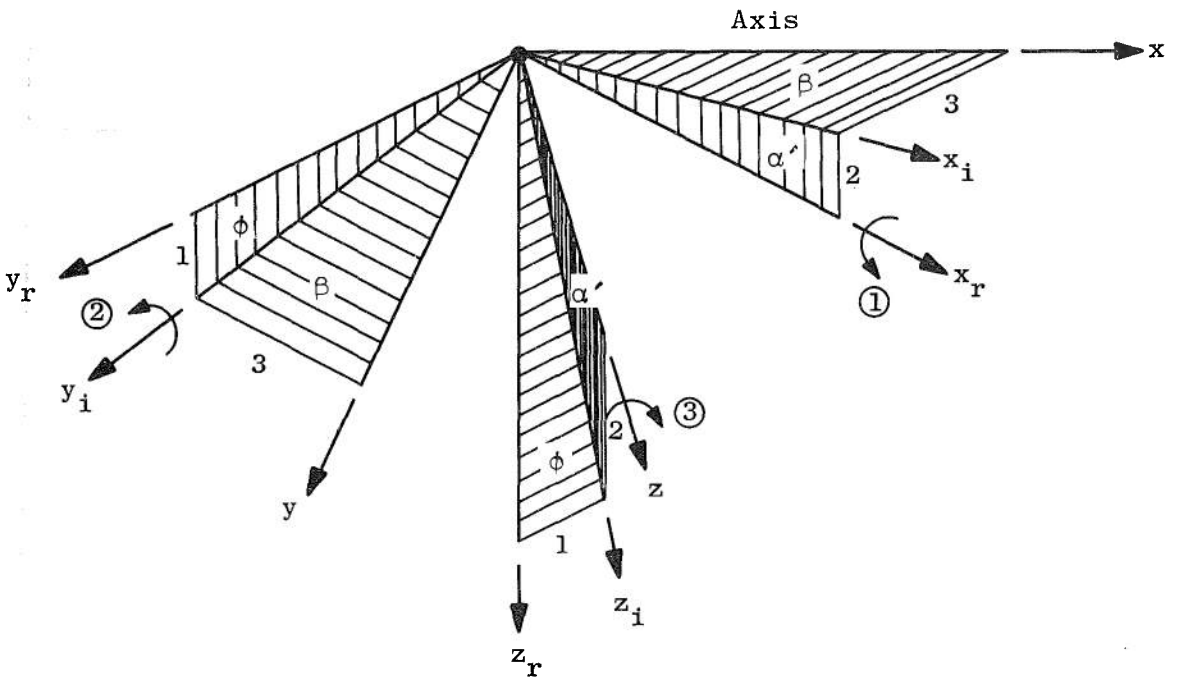

Fig. IV-6 Axis System

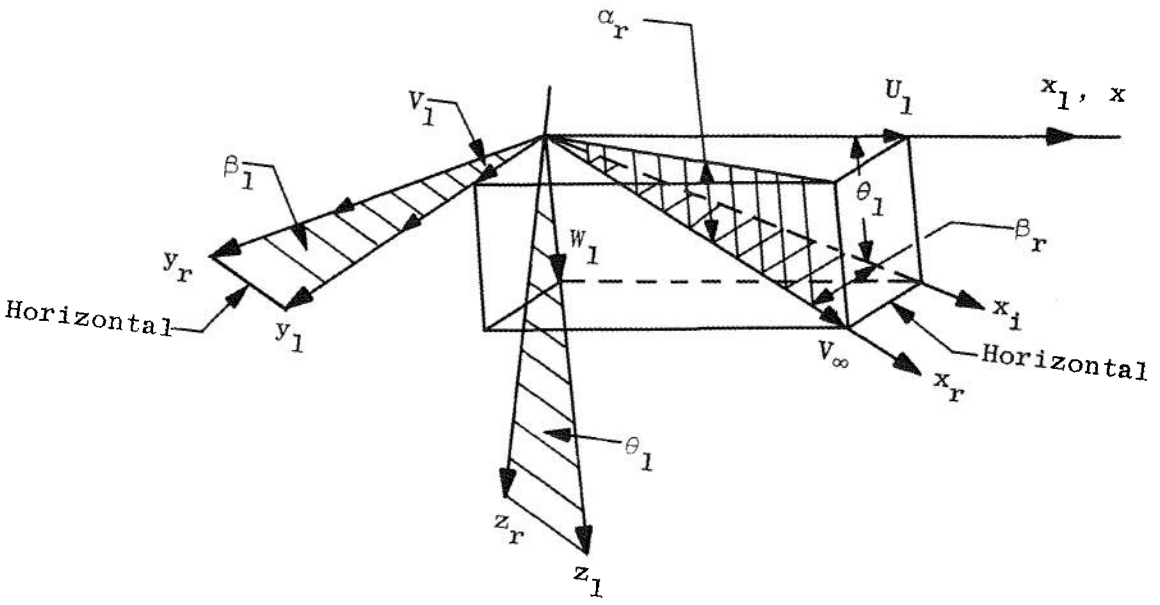

Fig. IV-7 Definition of Angles α_r and β_r

UNCLASSIFIED

Security Classification

DOCUMENT CONTROL DATA - R & D

(Security classification of title, body of abstract and indexing annotation must be entered when the overall report is classified)

1. ORIGINATING ACTIVITY *(Corporate author)*
Arnold Engineering Development Center
ARO, Inc., Operating Contractor
Arnold Air Force Station, Tennessee 37389

2a. REPORT SECURITY CLASSIFICATION
UNCLASSIFIED

2b. GROUP
N/A

3. REPORT TITLE
FREE-FLIGHT RANGE TESTS OF THE APOLLO COMMAND MODULE

4. DESCRIPTIVE NOTES *(Type of report and inclusive dates)*
January 25 to March 10, 1967 - Final Report

5. AUTHOR(S) *(First name, middle initial, last name)*
W. R. Lawrence and W. S. Norman, ARO, Inc.

6. REPORT DATE	7a. TOTAL NO. OF PAGES	7b. NO. OF REFS
January 1969	55	5

8a. CONTRACT OR GRANT NO.
F40600-69-C-0001

b. System 920E

c.

d

9a. ORIGINATOR'S REPORT NUMBER(S)
AEDC-TR-68-224

9b. OTHER REPORT NO(S) *(Any other numbers that may be assigned this report)*
N/A

10. DISTRIBUTION STATEMENT
This document has been approved for public release and sale; its distribution is unlimited.

11. SUPPLEMENTARY NOTES
Available in DDC.

12. SPONSORING MILITARY ACTIVITY
NASA, Manned Spacecraft Center,
Houston, Texas 77058

13. ABSTRACT

Results are presented for free-flight range tests of the basic Apollo Command Module configuration (smooth heat shield) conducted in Range G at nominal Mach numbers of 6.0 and 8.5. The Reynolds number based on model diameter and free-stream conditions varied from 50,000 to 240,000. Both drag and stability data are presented in addition to trim angles of attack corresponding to three lateral center-of-gravity positions. Comparison of the results with data from wind tunnels shows at most only small sting effects on the wind tunnel data.

DD FORM 1 NOV 65 1473

UNCLASSIFIED

Security Classification

14. KEY WORDS	LINK A		LINK B		LINK C	
	ROLE	WT	ROLE	WT	ROLE	WT
Apollo						
command module						
hypersonic flow						
wind tunnels						
aerodynamic drag						
aerodynamic stability						

AFSC
Arnold AFS Tenn